EVALUATION OF A MICROPLANE MODEL FOR

PROGRESSIVE FRACTURE IN CONCRETE

A Thesis

by

JAMES HARRIS LOPER

Submitted to the Graduate College of
Texas A&M University
in partial fulfillment of the requirements for the degree of

MASTER OF SCIENCE

December 1988

Major Subject: Civil Engineering

EVALUATION OF A MICROPLANE MODEL FOR

PROGRESSIVE FRACTURE IN CONCRETE
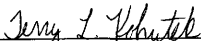
A Thesis

by

JAMES HARRIS LOPER
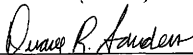
Approved as to style and content by:
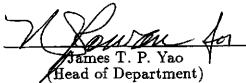
Ray W. James
(Chairman of Committee)

Jerry L. Kohutek
(Member)

James T. P. Yao
(Head of Department)

David H. Allen
(Member)

Duane R. Sanders
(Member)

December 1988

ABSTRACT

Evaluation of a Microplane Model for

Progressive Fracture in Concrete

(December 1988)

James Harris Loper, B.S., Texas A&M University

Chairman of Advisory Committee: Dr. Ray W. James

Tensile cracking of a concrete structure can affect its overall behavior considerably. The purpose of this study is to evaluate a microplane model for progressive tensile damage or fracture in concrete undergoing short term monotonic, plane stress load histories. The method of evaluation of the microplane model is in the form of a FORTRAN subroutine, which interfaces with the existing nonlinear finite element code ABAQUS, version 4.5. For cracked reinforced concrete, the smeared crack system is adopted. A strain criterion is used to quantitatively measure damage. The model is applied to unreinforced concrete subjected to uniaxial tension, biaxial tension, and pure shear. More realistic examples studied here are bending of a short, deep reinforced concrete shear panel and bending of a thin one–way reinforced concrete slab. Comparison between the plain concrete examples and experimental results shows good agreement. However, a good way of modeling tension stiffening is needed.

DEDICATION

For Mr. and Mrs. Jim Brown

ACKNOWLEDGEMENTS

I wish to extend my sincere appreciation to my chairman, Dr. R. W. James, for his advice and guidance during the course of this research. Also, I would also like to thank the other members of my research commitee, Dr. D. R. Sanders, Dr. D. H. Allen, and Dr. T. L. Kohutek.

Gratitude is also extended to my mother, Virginia, and brother, Alan, for their support throughout the years. In addition, I thank Mr. Joe Smith and Mr. Lee Medwick. Last, I thank Amy Wood for her open ears and fun–loving attitude throughout this research.

TABLE OF CONTENTS

LIST OF TABLES

LIST OF FIGURES

INTRODUCTION

Purpose and Motivation

Tensile cracking of a concrete structure can affect its overall behavior considerably. After starting at a relatively low tensile stress, tensile damage increases as tensile strain increases. As a result, the concrete exhibits strain softening, which is defined as a decrease in stress with increasing strain. A realistic constitutive model which accounts for the post–cracking regime or strain–softening region is an important part in the nonlinear analysis of concrete structures. The purpose of this study is to evaluate a microplane model for progressive tensile damage or fracture in concrete undergoing short term monotonic load histories.

The motivation of the present research lies in the need to evaluate the existing concrete constitutive models. Much attention has been given to the uniaxial tensile properties of concrete (Yankelevsky and Reinhardt 1987; Zhen–Hai and Xiu–Qin 1987; Reinhardt 1985; Gopalaratnam and Shah 1985; Krajcinovic 1983; Carino and Slate 1976; Tasuji, Slate, and Nilson 1978; Heilmann and Hilsdorf 1969; Evans and Marathe 1968; Newman 1968; Rosenthal 1968; Robinson 1967; Hughes and Chapman 1966; Hsu, Slate, Sturman, and Winter 1963; Weigler and Becker 1963; Nishizawa 1961; McHenry and Karni 1958; Blakely and Beresford 1955; Smith 1953). These test results laid the foundation for researchers to attack the problem of modeling concrete subjected to multiaxial stresses. Today, many computer codes exist which can model aspects of the behavior of concrete (Colville and Abbasi 1974; Bažant and Cedolin 1979; Bažant and Oh 1983A; Hibbitt 1985; Hillerborg 1985; Roelfstra and Wittman 1985 ; Gambarova and Floris 1986; Rashid and Dunham 1986). In order to effectively utilize any of these models, an understanding of

---

This thesis follows the format of the *Journal of Structural Engineering* of the American Society of Civil Engineers.

the scope and limitations of the model is needed. Here, one of the models, the microplane model, will be evaluated for plane stress cases.

Material Characteristics

The nature of the problem of modeling concrete behavior is highly nonlinear. Two reasons are responsible for this nonlinearity. The first cause is microdefects, which may result from shrinkage, temperature changes, discontinuities at the aggregate–mortar interface, segregation and bleeding, and discontinuities in the mortar due to capillary pores and inclusions (Mindness and Young 1981). Inhomogeneity of the material is the second cause of concrete's nonlinear behavior, Fig. 1. The stress–strain curves for the two main components of concrete are quite different as shown in Fig. 1, with both constituents being approximately linear except at stresses approaching the ultimate strength. The effect of this inhomogeneity is overall nonlinear behavior in a concrete body.

As a concrete body is subjected to external loads, it undergoes a fracture process which passes through three stages: crack initiation, slow crack growth, and rapid crack growth (Mindness and Young 1981). As shown in Fig. 2, concrete behavior in compression is nearly linear up to about 30% of the ultimate load. This linearity is due to the stability of pre-existing microcracks at low stress levels. The second stage of the fracture process includes two regions. First, between 30% and 50% of the ultimate strength, cracks at the aggregate-cement interfaces grow very slowly. Secondly, between 50% and 75% of the ultimate load, these interfacial cracks begin to extend into the cement matrix. The result is a more extensive and continuous crack system than at lower stress levels. From their experimental work, Carino and Slate (1976) defined a discontinuity point at about 70% of the ultimate load. This point is significant because it is appoximately the point where
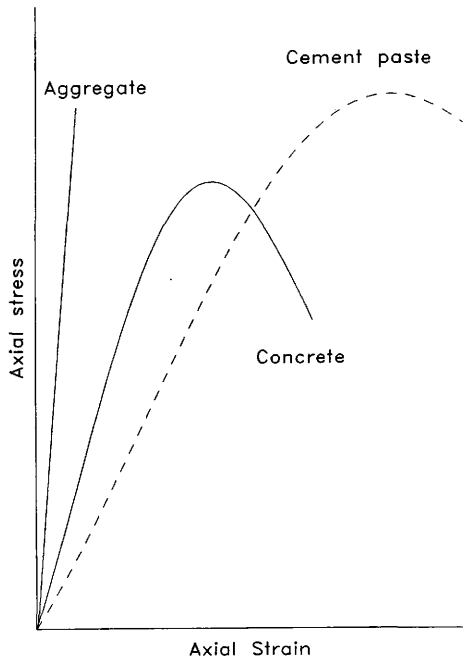
Fig. 1. Typical Stress−Strain Curves for Aggregate, Cement Paste, and Concrete (Mindness and Young 1981).
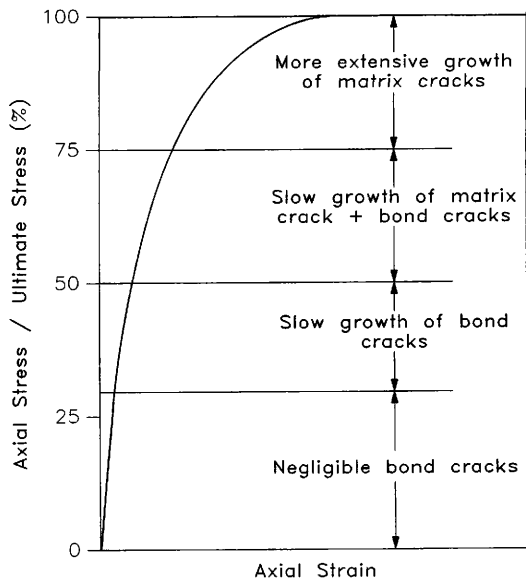
Fig. 2. Diagrammatic Stress–Strain Curve of Concrete in Compression (Mindness and Young 1981).

the curve deviates from linearity. The third stage of the fracture process occurs between 75% and 100% of the ultimate strength. Here, more extensive crack growth occurs in the matrix which leads to strain softening after the ultimate strength is reached. In contrast, Tasuji, Slate, and Nilson (1978) reported that the onset of major microcracking takes place at about 60% of the ultimate tensile stress. After the peak stress is reached, concrete exhibits strain softening. To observe the falling branch of the stress–strain curve, a stiff testing machine is needed which will prevent uncontrolled crack propagation and allow a constant strain rate to be maintained (Mindness and Young 1981).

Typical complete stress–strain curves for concrete under monotonic uniaxial compression are shown in Fig. 3 (Winter and Nilson 1979). The shape of the stress–strain curve is similiar for low, normal, and high–strength concretes, with the higher strength concretes exhibiting a slightly higher strain at the peak stress (Ramaley and McHenry 1947). In the strain–softening branch of the stress–strain curve, higher strength concretes tend to behave in a more brittle manner, with the stress decreasing more rapidly than in the case of lower strength concretes.

The initial modulus of elasticity, Young's modulus, of concrete is usually determined from an empirical relationship based on the concrete compressive strength, f'_c. The relation used by the ACI Building Code (ACI Code 318–83) is

$$E_c = 33\rho^{1.5}(f'_c)^{0.5}$$

where E_c = the initial compressive modulus in psi, ρ = unit weight in pcf, and E_c and f'_c are expressed in psi.

Poisson's ratio for concrete ranges from about 0.15 to 0.20, and is taken here
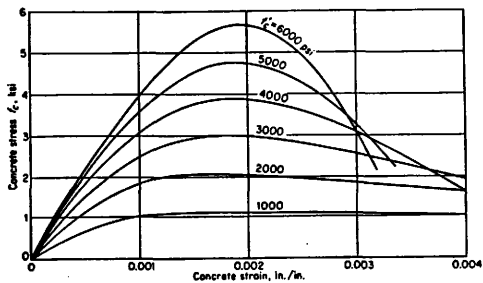
Fig. 3. Complete Stress—Strain Curves for Concrete in Uniaxial Compression (Winter and Nilson 1979). (1 ksi = 6895 kPa)

to be 0.18. At compressive stresses below about 80% of the peak stress, the ratio of lateral strains to longitudinal strains is constant, after which the apparent Poisson's ratio begins to increase. Incremental values of Poisson's ratio in excess of 1.0 have been measured (Darwin and Pecknold 1974, Kupfer, Hilsdorf, and Rüsch 1969).

When concrete undergoes cyclic compressive loading at stresses above about $0.60f'_c$, its stiffness degrades (Karsan and Jirsa 1969; Sinha, Gerstle, and Tulin 1964). As shown in Fig. 4 (Sinha et al. 1964), hysteresis curves are formed for each cycle of load. The area enclosed by each curve represents the energy dissipated by the concrete during that cycle. In a similiar study, Gopalaratnam and Shah (1985) showed that concrete subjected to cyclic tension also undergoes hysteretic effects.

Concrete subjected to uniaxial tension exhibits a stress–strain curve of similiar shape to that of compression loading, Fig. 5. However, the peak stress is much lower in tension than in compression. The ratio of tensile strength to compressive strength is about 0.1. Based on their experimental results, Tasuji, Slate, and Nilson (1978) suggested that the uniaxial tensile strength of concrete may be estimated from its uniaxial strength by

$$f_t = 6(f'_c)^{0.5}$$

The value taken by ACI for tensile strength is

$$f_t = 7.5(f'_c)^{0.5}$$

where f'_c is the compressive strength in psi. It is generally accepted that the strain corresponding to the maximum tensile stress is in the range of 50 to 150 micro–strains (Carino and Slate 1976; Jones 1968; Kaplan 1963).

As shown in Fig. 5, experimental results can vary greatly between researchers. The two main reasons for the differences in results are thought to be different
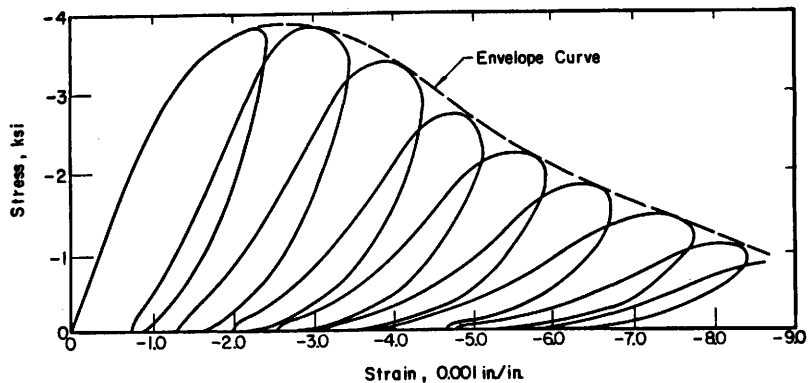
Fig. 4. Response of Concrete to Cyclic Uniaxial Compression
(Sinha et al. 1964).
(1 ksi = 6895 kPa)
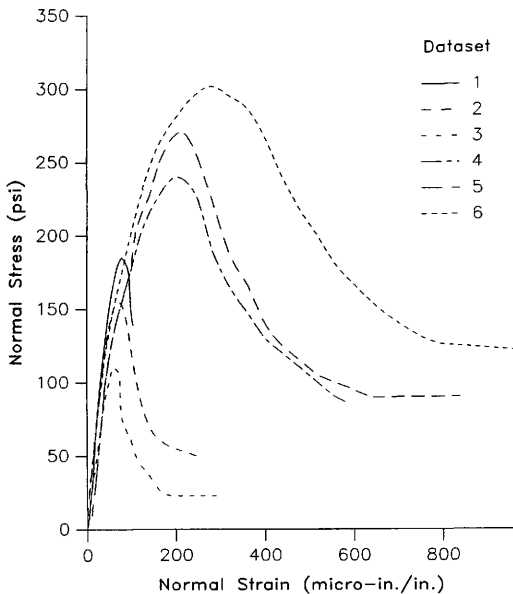
Fig. 5. Uniaxial Behavior of Concrete in Tension (Hughes and Chapman 1966; Evans and Marathe 1968).
(1 psi = 6.895 kPa)

material mix proportions and different experimental test procedures used by the researchers, Table 1. Even though the ages and water–to–cement ratios were similiar, the coarse aggregate–to–cement ratios differed between the workers. Further, the maximum aggregate size used by Evans and Marathe (1968) was not given. In addition to material differences, another reason for the dissimiliarities is the difference in test procedures used in the tests. Rüsch (1960) showed that the applied strain rate considerably affects the compressive results, Fig. 6. The same phenomenon is a possibly a cause of contrast in this case. Also, if the testing machines' stiffnesses differed greatly, then the different strain energies stored in each machine could lead to different results. To guarantee a controllable strain rate in the strain-softening region, a stiff testing machine is needed, else the results will indicate that concrete is essentially an elastic–brittle material. Work by other researchers (Tasuji, Slate, and Nilson 1978; Carino and Slate 1976) supports the idea that a soft testing apparatus greatly shortens the period of slow crack growth, and leads to failure almost immediately after the first crack developes.

Several modeling problems arise from the nature of concrete. First, material heterogeneity and nonlinearity cause problems in explaining experimental results and extrapolating them (Carpinteri 1982). Further, on the uniaxial stress–strain diagram, any stress less than f_t, the maximum tensile stress, corresponds to two strains. In addition, concrete micro–cracking causes the stress state within the body to be nonhomogeneous. Also, the effects of creep and shrinkage create complications. If the concrete is reinforced, bond slip between the steel and concrete cause problems in modeling.

Method of Evaluation

The method of evaluation of the microplane model will be in the form of
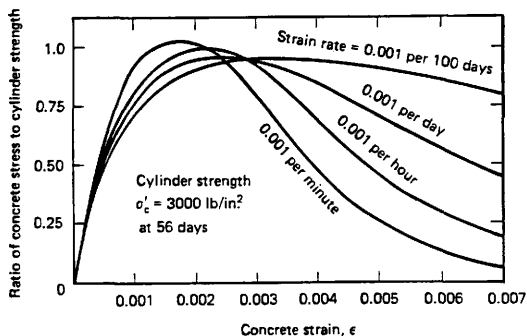
Fig. 6. Strain–Rate Effect on Uniaxial Compressive Response (Rüsch 1960). (1 psi = 6.895 kPa)

Table 1. Material Properties for Data in Fig. 5.

Dataset[1] (1)	Age (days) (2)	w/c[2] (3)	CA/Cem[3] (4)	Max Agg Size (5)	$\dot{\epsilon}$ (μ/min) (6)
1	60	0.45	2	$\frac{3}{8}$	4
2	90	0.45	2	$\frac{3}{16}$	4
3	31	0.45	2	$\frac{3}{8}$	4
4	31	0.45	3	N/A	10
5	42	0.45	3	N/A	10
6	105	0.45	3	N/A	10

(1) Datasets 1, 2, and 3 are by Hughes and Chapman (1966), and

datasets 4, 5, and 6 are by Evans and Marathe (1968).

(2) water/cement ratio by weight.

(3) Coarse aggregate/cement ratio by weight.

a FORTRAN subroutine. The subroutine will be based on Bažant's proposal (Bažant and Oh 1983A; Bažant 1984; Bažant and Gambarova 1984; Bažant and Oh 1985). First, constitutive relations from the microplane model will be generated. From these constitutive relations, an algorithm will be developed and coded into a FORTRAN subroutine. The FORTRAN subroutine will interface with the existing nonlinear finite element code ABAQUS. Concrete structures subjected to plane stress states will be studied. Examples to be considered are the two–dimensional cases of uniaxial and biaxial tension of a plane stress element, the bending of a shear–beam, and the bending of a one–way reinforced slab. The initiation and growth of tensile cracks in these structures will be studied. Here, progressive damage or

growth of tensile cracks is defined simply by increasing strains on microplanes. Growth of single cracks, which may be modeled by fracture mechanics, is not considered. Results of the numerical analysis will be compared with available experimental data (Gambarova and Floris 1986, Bažant and Oh 1985, Jain and Kennedy 1974). The comparison will be based on the magnitude of loads that cause cracking and the locations and orientations of the cracks. Further comparisions will be made between experimental and analytical results with regard to load–displacement curves. Limited studies of convergence and numerical instability with the chosen constitutive model will be reported.

REVIEW OF THE LITERATURE

Continuum Damage Mechanics

The idea of continuum damage mechanics (CDM) originated in 1958, when Kachanov introduced a kinematic variable defining the microdefect density in a body. Kachanov's work was motivated by his realization of the difference in effect that microcrack growth and dislocation kinetics have on the creep of metals. The results of Kachanov's work led to modern day continuum damage mechanics, a branch of continuum solid mechanics characterized by the introduction of special internal field variables representing the distribution of damage locally (Krajcinovic 1984). In this study, continuum damage mechanics is defined as branch of the damage mechanics in which no boundary conditions are imposed on the interior a body. Examples of such boundary conditions are voids and cracks.

In the present state of the art, CDM is a controversial topic, because damage can be described in many ways. For examples, the damage laws can be developed from either a state type or a memory type of theory. In the state type of theory, the history of the body does not need to be known, because a set of internal state variables are available to characterize the state at any time. In contrast, the entire history of the body must be known, in a memory type of theory. Another source of controversy in CDM is the damage tensor order to be used. The damage tensor can be of any order, Table 2 (Krajcinovic 1984).

As stated by Krajcinovic (1984), some of the major contributors to damage mechanics research of spalling, brittle materials are Davison and Stevens (1973), Curran (1973), Chaboche (1978), Dragon and Mróz (1979), Krajcinovic and Fonseka (1981), and Murakami and Ohno (1981). All of the theories proposed by these researchers, with the exception of Curran's, employ an evolution equation or a

Table 2. General CDM Theories[1].

Original Reference (1)	Damage Tensor Order[2] (2)	Damage Law[3] (3)
Davison, Stevens 1973	1	EE
Chaboche 1978	8	EE
Dragon, Mróz 1979	2	FP
Krajcinovic, Fonseka 1981	2	FP
Murakami, Ohno 1981	2	EE

(1) Only theories incorporating the damage variable explicitly are listed.

(2) Scalar and vector tensors are of order 0 and 1.

(3) EE-evolution law, FP-Flow potential

flow potential. Curran's theory is not a continuum mechanics type theory because damage is obtained by integrating over a sphere surrounding a material point. In contrast to these researchers, another group, including Rudnicki and Rice (1975), Doughill (1975), Bažant and Kim (1979), and Nicholson (1980), characterized the damage indirectly through an additional component of the strain tensor (cited in Krajcinovic 1984). In addition to Chang and Allen (1987) and Allen and Harris (1987), other contributors to damage mechanics include Lemaitre (1971), Leckie (1974), Hult (1974), and Chaboche (1974) (cited in Lemaitre 1984).

Another continuum damage mechanics model, the microplane model, was proposed by Bažant and Oh (1983A). Their objective was to model damage in brittle aggregate materials such as concrete. They approached the objective with a micromechanics perspective.

Non–Continuum Damage Mechanics

For certain materials, CDM cannot be used due to large amounts of inhomogeneity. In such cases, a non–continuum approach must be used to realistically model damage effects. Seaman, Curran, and Shockley (1976) developed a non–continuum damage mechanics model for fracture criteria of various metals. Their main objective was to develop the capability to predict quantitatively the level of damage produced under known dynamic loads. Damage was obtained over a sphere surrounding a material point.

Damage in Concrete

Progressive Crack Growth

Presently, two approaches are available to quantify tensile damage or crack growth in concrete. These are discrete crack formulation, proposed by Griffith (Krajcinovic 1979), and the smeared crack formulation, proposed by Kachanov (1958) and Rashid (1968). Griffith's formulation is based on growth and propagation of a single crack. Kachanov's proposal is based on damaged smeared over a volume of material. The smeared damage approach, utilized by Bažant and Cedolin (1980), Cervenka and Gerstle (1972), Suidan and Schnobrich (1973), and Darwin and Pecknold (1976), has gained favor over the discrete crack approach for two reasons. First, a material such as concrete is commonly characterized by many cracks of various sizes and orientations in a tensile zone. This fact makes the smeared crack model attractive because one pays no penalty for lack of apriori knowledge of crack sizes and orientations. The second advantage of the smeared model is its relatively simple installation into a finite element program. The extent of damage can be simulated by decreasing the element stiffnesses rather than by introducing gaps in the finite element mesh as required in the case of discrete crack growth models.

A third approach, fracture mechanics, may be used to quantify crack propagation if locations and extent of initial cracks are known. This method has been met with mixed reviews because some researchers (Kesler, Naus, and Lott 1972) feel it is impractical while others (Bažant ant Cedolin 1980) feel there is no other way besides fracture mechanics to achieve what they consider an objective approach to the crack propagation problem.

Concrete Failure Theories

Probably the first criterion for the onset of plastic deformation in hydrostatic dependent media was proposed by Coulomb in 1773 when he was studying the interaction between soil and retaining walls. His work laid the foundation for became known as the Mohr–Coulomb theory. Then in 1864, Tresca, who is credited as being the father of plasticity, developed a yield criterion which assumes the onset of yielding is due to shear stress or distortional energy instead of normal stress or dilatational energy. Rankine followed with his maximum stress theory in 1876. He assumed that failure occurs when the normal stress in any direction exceeds a limiting value.

Two of the best known concrete failure models are the Mohr–Coulomb model and the Drucker–Prager model. The Mohr–Coulomb theory assumes failure occurs on a plane when the shear stress τ reaches a limiting value. The limiting value of τ is a function of confining pressure or compressive normal stress on that plane.

$$\tau = f(\sigma_n)$$

Using a straight line approximation, the maximum stress is given by

$$\tau = c + \sigma_n \ tan\phi$$

where ϕ = the angle of internal friction and c = cohesion. Any state of stress whose Mohr's circle falls inside the failure envelope is assumed to behave in an elastic manner, Fig. 7.

The Drucker-Prager model is a linear, mean stress dependent yield function which takes on the shape of a cone in principal stress space. The function f, defining yield, is given by

$$f = 3\alpha I_1 + (J_2)^{\frac{1}{2}} - k = 0$$

where

$$\alpha = \frac{2 sin\phi}{3(3 - sin\phi)}$$

$$k = \frac{2 cos\phi}{(3 - sin\phi)}$$

$$I_1 = \sigma_{kk}$$

$$J_2 = \frac{1}{2}\sigma'_{ij}\sigma'_{ij}$$

$$\sigma'_{ij} = \text{ deviatoric stress tensor}$$

The Mohr–Coulomb and Drucker–Prager models are the basis for more recent models. One such model, proposed by Kupfer and Gerstle (1973) and widely accepted, is shown in Fig. 8. Here, the failure surface is expressed individually for the regions of biaxial tension, tension–compression, and biaxial compression. Other recent concrete failure theories include those by Argyris, Faust, Szimmat, Warnke, and Willam 1974; Kotsovos and Newman, 1978; Ottosen 1977; and Willam and Warnke 1974.
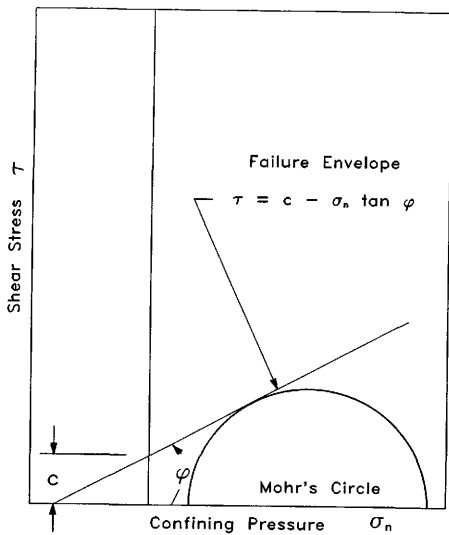
Fig. 7. Mohr–Coulomb Failure Theory.
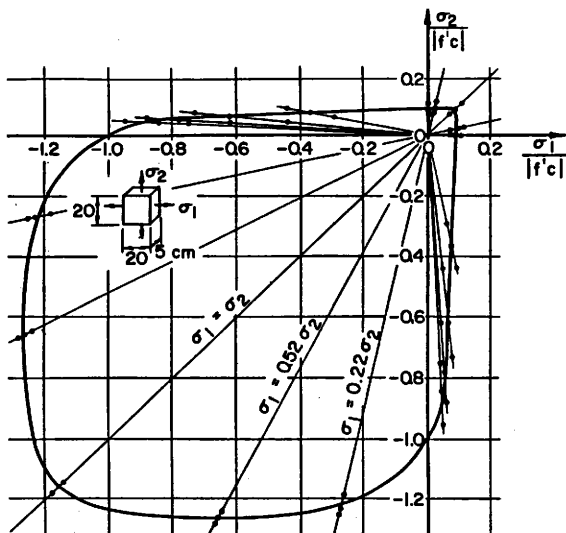
Fig. 8. Biaxial Strength of Concrete (Kupfer and Gerstle 1969).
(2.54 cm = 1 in.)

Concrete Constitutive Relations

Elasticity–Based Models

In the earliest concrete finite element models, the material was considered to be linear elastic and isotropic. Hookean formulations, involving either total or incremental stress–strain relations, were used to model biaxial concrete behavior. In such models, the expression for the stress is function of strain only:

$$\sigma_{ij} = F_{ij}(\epsilon_{ij})$$

where F_{ij} = tensorial material response function. Specifically, the stress–strain relation is

$$d\sigma_{ij} = D_{ijkl} \ d\epsilon_{kl}$$

where D_{ijkl} = a fourth-order material stiffness matrix.

Linear material modeling of concrete began with research on uniaxial domains (Aktan and Pecknold 1975; Blakely and Park 1973; Karsan and Jirsa 1969, Kent and Park 1971; Sinha, Gerstle, and Tulin 1964; Suharwardy and Pecknold 1978) and soon progressed to biaxial (Ngo and Scordelis 1967; Rashid 1968) and triaxial (Cedolin, Crutzen, and Dei Poli 1977; Kotsovos and Newman 1978; Ottosen 1979; Palaniswamy and Shah 1974; Phillips and Zienkiewicz 1976) models. The advantage of these models is that no loading functions, flow rules, or intrinsic time are required. However, because concrete is a highly nonlinear material, more complex models were destined to follow.

Classical Plasticity–Based Models

With the desire to more realistically model concrete came models based on classical plasticity theory, where concrete is assumed to be a stable material. A stable material is defined to be one in which the plastic work done by the tractions

during any load step is positive (Malvern 1969). In addition to this assumption, researchers further make one of two other simplifying assumptions. First, concrete may be assumed to be an elastic–perfectly plastic material, which can flow like a ductile metal on the yield surface. Second, concrete may be assumed to be a strain-hardening or work-hardening material, in which the net total work done by the tractions during the cycle of adding and removing stresses is nonnegative. In classical plasticity, the idea of strain softening is precluded, because all tensile strength is assumed to be lost after an ultimate tensile stress is reached. Several researchers (Chen 1981; Chen and Ting 1980; Buyukozturk 1977; Chen and Chen 1975) have proposed such models, using either isotropic, kinematic, or combined hardening rules in their respective formulations. An extension of the model by Chen and Chen (1975) was reported by Hibbitt (1985), in an effort to make the model more realistic by including a strain failure criterion.

The advantage of classical plasticity–based models is that such models incorporate nonlinearity of concrete. One disadvantage is that the material strength of concrete may be overestimated because yielding in compression is assumed to be independent of hydrostatic pressure. To avoid the overestimation of strength, the yield surface may be capped. Another disadvantage is strain softening is not modeled.

In classical plasticity theory, the four main topics to be considered are the stress–elastic strain relation, the yield criterion, the flow rule, and the work–hardening rule. These subjects are summarized as follows.

A. Stress–Elastic Strain Relation

$$d\sigma_{ij} = D_{ijkm} d\epsilon_{ij}^{El}$$

where $d\epsilon_{ij}^{El} = d\epsilon - d\epsilon_{ij}^{Pl}$,

and $d\epsilon_{ij}^{El}, d\epsilon$, and $d\epsilon_{ij}^{Pl}$ are the elastic, total, and plastic strain increments, respectively.

D_{ijkm} = the incremental stiffnesses.

B. Yield Criterion

$$F(\sigma_{ij}) = 0$$

C. Flow Rule

$$d\epsilon_{ij}^{Pl} = d\lambda \frac{\partial F}{\partial \sigma_{ij}}$$

where λ = a history dependent scalar.

D. Work–Hardening Rules

The purpose of the work–hardening rule is to describe the growth of all internal state variables (ISV) in the formulation. For combined hardening, the work–hardening rules are

$$d\alpha_2 = H' d\bar{\epsilon}^{Pl}$$

where α_2 = drag stress, which describes the growth of the yield surface.

$H' = d\sigma d\bar{\epsilon}^{Pl}$ = work hardening modulus

$d\bar{\epsilon}^{Pl} = \left(\frac{2}{3} d\epsilon_{ij}^{Pl} d\epsilon_{ij}^{Pl}\right)^{1/2}$

$$d\alpha_{3ij} = d\mu(\sigma_{ij} - \alpha_{3ij})$$

α_{3ij} = back stress, which describes the yield surface translation.

Plastic–Fracturing Model

In another effort to more realistically model concrete behavior, Bažant and Kim (1979) proposed the plastic–fracturing model. Plasticity theory is driven by plastic slip of planes in a body. In concrete, much of the inelastic behavior may be attributed to microcracking. This model quantifies the inelastic strain contributed to a body by microcracking, and adds it to the inelastic strain contributed by

plastic slip in the body. Specifically, two loading surfaces are defined. From these loading surfaces, the plastic strain increment and the fracturing stress decrement are determined. The plastic strain increment is defined, as in classical plasticity theory, by the flow rule. The fracturing stress decrement is determined from Iliushin's postulate and represents a decrease in stress due to concrete fracturing.

The distinction between a plastic material and fracturing material is important here because it is combination of these two that is the basis of the model. A plastic material is one in which macroscopic inelastic behavior is governed by plastic slip at the microscopic level. Graphically, a plastic material behaves uniaxially as shown in Fig. 9 (Bažant 1980).

The second-order work done during the infinitesimal cycle of adding and removing $d\sigma_{ij}$ is

$$\Delta W = \frac{1}{2} d\sigma_{ij} d\epsilon_{ij}^{Pl} \geq 0$$

which is Helmoltz's free energy in the case of isothermal conditions. It is also a representation of Drucker's postulate. If $\Delta W \geq 0$, work must be supplied to produce deformation. This condition ensures stability of the material. If $\Delta W < 0$, work is released or available during the deformation. Even though this condition implies material instability through a violation of Drucker's postulate, overall stability may still be maintained.

A fracturing material is one in which inelastic behavior is governed by micro-cracking and void formations at the microscopic level. Graphically, a fracturing material behaves uniaxially as shown in Fig. 10 (Bažant 1980).

The second-order complementary work done during the infinitesimal cycle in which the strain $d\epsilon_{ij}$ is superimposed and removed is

$$\Delta \pi = \frac{1}{2} d\epsilon_{ij} d\sigma_{ij}^{Fr} \geq 0$$
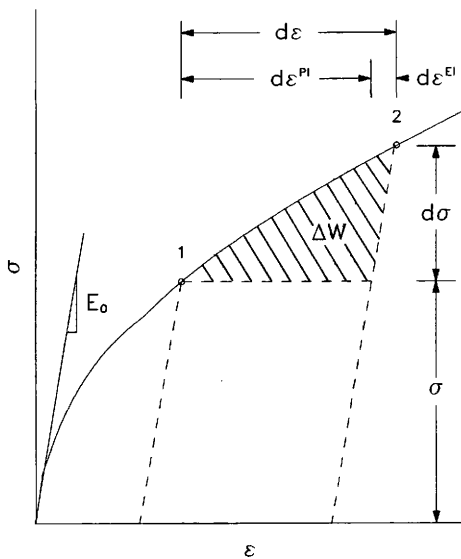
Fig. 9. Uniaxial Behavior of a Plastic Material (Bažant 1980).
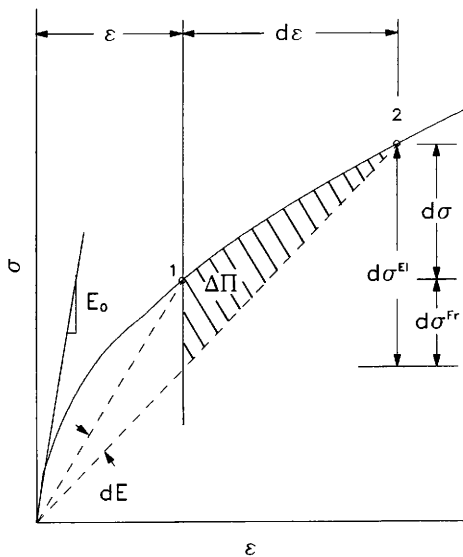
Fig. 10. Uniaxial Behavior of a Fracturing Material (Bažant 1980).

$\Delta\pi$ is Gibb's free energy and a representation of Iliushin's postulate. The stress decrement is $d\sigma_{ij}^{Fr}$. If $\Delta\pi \geq 0$, work must be supplied to produce deformation. If $\Delta\pi < 0$, the material may or may not be stable due to the work made available by the body.

A plastic–fracturing material is one in which the inelastic behavior is characterized by plastic strain increments $d\epsilon_{ij}^{Pl}$ and fracturing stress decrements $d\sigma_{ij}^{Fr}$. Graphically, a plastic–fracturing material behaves uniaxially as shown in Fig. 11 (Bažant 1980).

The work done during a infinitesimal load cycle is

$$\Delta U = \frac{1}{2}(d\sigma_{ij}d\epsilon_{ij}^{Pl} + d\sigma_{ij}^{Fr}d\epsilon_{ij}) \geq 0$$

It is assumed that this equation holds for the special cases when either $d\epsilon_{ij}^{Pl}$ or $d\sigma_{ij}^{Fr}$ are zero and for the general case when neither is zero.

Possibly the best way to understand this model is to directly compare it with classical plasticity theory. The main parts of the theory, as described by Bažant (1980), are summarized as follows.

A. Stress–Elastic Strain Relation

$$d\sigma_{ij}^{El} = D_{ijkm}d\epsilon_{km}^{El}$$

where $d\epsilon_{km}^{El} = d\epsilon_{km} - d\epsilon_{km}^{Pl}$

$d\sigma_{ij} = d\sigma_{ij}^{El} - d\sigma_{ij}^{Fr}$ and

$d\sigma_{ij}^{Fr} = (dD_{ijkm})d\epsilon_{km}$

Thus, we have

$$d\sigma_{ij} - (dD_{ijkm})d\epsilon_{km} = D_{ijkm}(d\epsilon_{km} - d\epsilon_{km}^{Pl})$$

The uniaxial form of these equations is

$$d\sigma_{11} = E(d\epsilon_{11} - d\epsilon_{11}^{Pl}) + d\epsilon_{11}dE$$
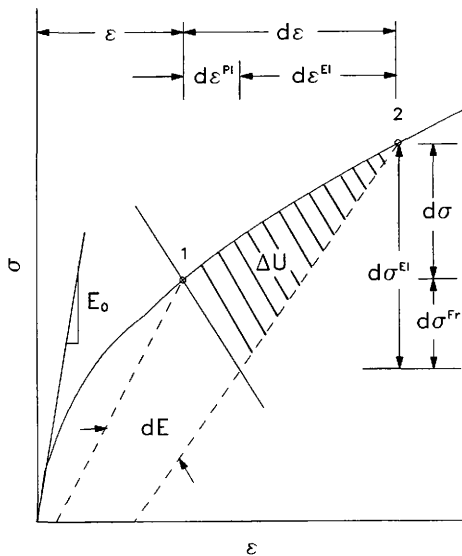
Fig. 11. Uniaxial Behavior of a Plastic-
Fracturing Material (Bažant 1980).

B. Yield Functions

    1) Plastic Load Function

$$F = F(\sigma_{ij}, H_k) = 0$$

where H_k = The fracture tensor and is a set of N ISV, which may contain ϵ_{ij}.

    2) Fracturing Load Function $\Phi = \Phi(\epsilon_{ij}, H'_k) = 0$

where H'_k = a set of M ISV, which may contain σ_{ij}.

C. Flow Rules

    1) Plastic Flow Rule or Normality Rule in Stress Space

$$d\epsilon_{ij}^{Pl} = d\lambda \frac{\partial F}{\partial \sigma_{ij}}$$

where $d\lambda = \frac{1}{h} \frac{\partial F}{\partial \sigma_{km}} d\sigma_{km}$ and

h = a scalar called the normal plastic modulus

$h = h(\sigma_{ij}, \epsilon_{ij})$

2) Fracturing Rule or Nomality Rule in Strain Space

$$d\sigma_{ij}^{Fr} = d\kappa \frac{\partial \Phi}{\partial \epsilon_{ij}}$$

κ = a scalar called the normal plastic modulus $\kappa = \kappa(\sigma_{ij}, \epsilon_{ij})$

D. Growth Laws

    Taking the time derivatives of the plastic and fracturing flow rules,

$$\dot{\epsilon}_{ij}^{Pl} = \dot{\lambda} \frac{\partial F}{\partial \sigma_{ij}} \qquad \dot{\sigma}_{ij}^{Fr} = \dot{\kappa} \frac{\partial \Phi}{\epsilon_{ij}}$$

The rates of growth of the fracture and hardening parameters are

$$\dot{\lambda} = \Phi_1(X) \qquad \dot{\kappa} = \Phi_2(Y)$$

where

$$X = \frac{\partial F}{\partial \sigma_{km}} \dot{\sigma}_{km} \qquad Y = \frac{\partial \Phi}{\partial \epsilon_{km}} \dot{\epsilon}_{km}$$

and Φ_1, Φ_2 are continuous, smooth, and monotonically increasing functions.

In the plastic–fracturing model, the normality condition is relaxed. Specifically, the plastic strain increment is not required to be normal to the yield surface. The reason for this relaxation is the type of inelastic behavior of geomaterials. At the microstructural level, normality holds for perfectly plastic slip, as exhibited by metals, but not for frictional slip. Frictional slip is characterized by microcracking or formation of voids, which is typical for rocks, soils, and concretes.

Two load functions are defined in the model. The first of them accounts for plastic strains in which no change in elastic moduli occurs. The second accounts for fracturing stress decrements, which are caused by a degradation of elastic moduli. Any unloading is assumed to be elastic but with reduced moduli.

The main difference between classical plasticity and plastic–fracturing model is manifested in the idea that inelastic behavior in geomaterials is driven not only by slip planes, as in metals, but also by microcracking and void formations. It is this major difference between metals and geomaterials that requires a model which accounts for the stress decrements caused by microcracking and void formations. The plastic–fracturing model is relatively new, and because it has not been used to fit test data to a large extent, it has not been proven to be an efficient concrete model.

In a separate study, Dragon and Mróz (1979) proposed another continuum model for plastic–brittle behavior of rock and concrete. Their model is almost identical to the plastic–fracturing model proposed by Bažant. Both models are clearly based on and are extensions of the work by Doughill (1975, 1976), who first

introduced the fracturing load function, for a purely fracturing material.

Endochronic Theory

Possibly the most complicated concrete constitutive models are based on the endochronic theory. This theory uses reduced time, z, which is intrinsically related to the deformation of the material.

The simplest form of this theory was developed by Valanis in 1971, and can be derived from thermodynamic concepts (Allen 1988). In 1968, Schapery observed that the endochronic theory is a special case of visco–plasticity with a strain–rate dependent viscosity. It has been utilized by several researchers (Bažant and Shieh 1978; De Villiers 1977; Hsieh 1980; Sorenson, Arneson, and Bergan 1978; Fanning and Dodge 1979), and it has the advantage of being a more realistic and comprehensive representation of inelastic behavior than previous models.

After laying the thermodynamic foundations, Valanis arrived at the multiaxial form of the stress–strain relation

$$\sigma_{ij} = 2 \int_{z_0}^{z} \mu(z - z') \frac{\partial \epsilon_{ij}}{\partial z'} dz'$$

$$\sigma_{kk} = K \epsilon_{kk}$$

where K = Bulk Modulus of the material,

z_0 and z = Initial and final intrinsic times in a load step, respectively, and

$z_0 \leq z' \leq z$

The function $\mu(z - z')$ may consist of a single exponential term such as

$$\mu(z) = \mu_0 e^{-\alpha z}$$

or a multiple exponential term such as

$$\mu(z) = \mu_0 + \mu_1 e^{-\alpha z}$$

where $\mu_0 + \mu_1$ = the shear modulus at z = 0, and α = a constant.

If the single exponential term is used, and plastic incompressibility is assumed, the multiaxial form of the theory becomes

$$\sigma_{ij} = 2\mu_0 \int_{z_0}^{z} e^{-\alpha(z-z')} d\epsilon_{ij}(z')$$

which may be reduced to the differential equation

$$d\epsilon_{ij} = \frac{\alpha}{2\mu_0} dz \sigma_{ij} + \frac{1}{2\mu_0} d\sigma_{ij}$$

and is equal to the deviatoric form of the Prandtl–Reuss equations.

The Microplane Model

The microplane model was first developed by Bažant and Oh (1983A) to model brittle aggregate materials such as concrete and rock. The main idea of this model is to first determine the inelastic behavior of each microplane or "weak plane" (Gambarova and Floris 1986), and then use the principle of superposition to obtain the overall inelastic behavior of a body. This idea can be traced back to the work of Taylor (1938), who applied it to the plasticity of polycrystalline metals. Then, in 1949, Batdorf and Budiansky formulated the slip theory of plasticity, in which the stresses acting on various slip planes are assumed to be resolved components of the macroscopic applied stress tensor, and the plastic strains from all slip planes are superimposed. Como and D'Agostino (1969) extended the slip plane concept to the analysis of metals exhibiting strain hardening. Calladine (1971), using an approach similiar to the slip plane idea, analyzed saturated clay. He considered the clay to be as crisscrossed by "contact planes", where each contact plane is free to close up and slip according to the history of the normal and shearing stresses acting on it. The assumption of kinematic independence of each plane differentiates the

behavior of porous materials like saturated clay and concrete from metals, where displacements of different planes should not be independent of each other (Wu and Drucker 1967).

In 1977, Zienkiewicz and Pande proposed a multilaminate model for rocks and rock–like materials with multiple planes of weakness. The model specified an elastic–plastic constitutive relationship for the shear stress and shear strain, and a purely elastic relationship for the normal stress and normal strain, with no tensile strength.

The microplane model (Bažant and Oh 1983A) was developed to describe progressive tensile fracture of concrete. It is based on a local view, superposition of inelastic behavior on all microplanes at a point in a body, in contrast to a global view, direct description of a body's macroscopic behavior. The reason for using a local view approach is that microcracking is assumed to be localized in the thin mortar layers which separate the coarse aggregate particles.

In the microplane model, damage may be assumed to be anything from isotropic to fully anisotropic. The key to characterizing the anisotropic damage of the material is a special function, which is the normalized frequency distribution of microplanes of various orientations. The function weights some microplanes more heavily than others in the averaging process, which determines the tangent stiffness matrix during each load step. This averaging process quantifies the damage at each material point by integration over a unit hemisphere for three–dimensional problems or over a unit semicircle for plane problems. The model has been applied to reinforced concrete shear walls (Donida, Floris, and Gambarova 1987), hollow cylinders subjected to axial compression and torque (Gambarova and Floris 1986), and anisotropic creep of clay (Bažant 1984).

INTRODUCTION TO DAMAGE MECHANICS

Damage is defined as the decrease in strength of engineering materials due to microstructural changes caused by mechanical and environmental conditions (Kachanov 1986). It is an irreversible or dissipative phenomenon in which entropy increases. In his work, Kachanov (1986) discussed seven major categories of damage. The first group is creep damage, which is characterized by microvoids in metal grains and/or microcracks on intergranular boundaries. Creep damage can occur at high temperatures and moderate stresses. The second category of damage is ductile plastic damage, in which large plastic strains cause an accumulation of microvoids in grains and micocracks at the intergranular boundaries. The third class of damage is fatigue damage. Under cyclic loading, the structure gradually deteriorates because of accumulation and growth of micro and macro cracks. The fourth division is embrittlement of steels, in which steel undergoes a decrease in plasticity due to restructuring. It can be caused by atomic radiation, and causes steel to become brittle. An example of steel embrittlement is hydrogen brittleness, where hydrogen atoms diffuse into the steel atomic grid, causing dislocations. The fifth category of damage is chemo–mechanical damage or stress corrosion. Here, galvonic corrosion is accelerated by the presence of stresses. Environmental degradation, the change in the mechanical properties due to environmental attack, is the sixth category of damage. Examples of materials susceptible to environmental damage are soils, geo–materials, polymers, and wood. This type of damage may occur without any applied stress on the body. The seventh category of damage is damage of concrete, where cracks appear under loading due to weak zones in a heterogeneous media.

Damage can occur in one of three ways: elastic deformation, elastic–plastic deformation, and creep. An example of damage of a body under elastic deformation is

high–cycle fatigue. Examples of damage of a body under elastic–plastic deformation are ductile plastic damage and low–cycle fatigue.

In 1958, Kachanov (Lemaitre 1984) introduced a continuous variable related to the density of micro–cracks and cavities in a body. This variable has constitutive equations for evolution of microcracks and cavities, written in terms of stress or strain which can be used in structural analysis to predict the initiation of microcracks. Researchers Lemaitre (1971), Leckie and Hayhurst (1974), Hult (1974), and Chaboche (1974) formulated these constitutive equations in the framework of thermodynamics and identified many phenomena, including the three main modes of damage discussed above (cited in Lemaitre 1984). As a result of these efforts, damage mechanics has now reached a state of development which allows engineering application.

Damage Variable

In a damaged body, consider a volume element at macro–scale, that is of large enough size to contain many defects, and small enough to be considered as a material point in the mechanics of a continuum, Fig. 12. A damage variable w is needed to quantify the damage in the body. Define w as the set of all parameters describing the damage. No damage exists if $w = 0$.

$$\text{Then} \quad \dot{w} = \dot{w}(\sigma_{ij}, w, ...)$$

where

$$\dot{w} = \frac{dw}{d\lambda}$$

λ = Monotonically increasing parameter similiar to time. For irreversible processes, λ is related to the entropy of the body.

The choice of the function of w may be based on physical microstructural analysis or direct generalization of experimental data. In its simplest form, the
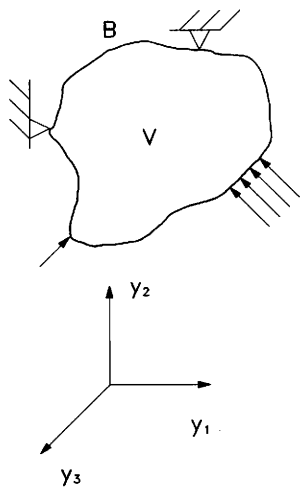
Fig. 12. A Continuous Domain.

damage variable is a scalar, as proposed by Kachanov (1958). As shown by Krajcinovic (1984), the main damage mechanics theories at present use damage tensors ranging in order from 0 to 8. In addition to these theories, Cordebois and Sidoroff (1982) introduced a fully anisotropic law involving 21 independent components. Also, Tamuzh and Lagsdinsh (1968) proposed a model in which damage is described by a set of functions given on the surface of a unit sphere surrounding an arbitrary point in a body.

As a simple damage mechanics model, consider uniaxial stress of the damaged body in Fig. 13. Let A_0 be the undamaged increment of area, dS, and A be the damaged area. For the special case of isotropic damage, in which damage is assumed to be the same in all directions, w is a scalar.

$$w = \frac{A}{A_0} \qquad 0 < w < 1$$

where w is a positive and monotonically increasing function. For metals, the critical value of w is between 0.2 and 0.8 (Lemaitre 1984). The effective stress vector, $\overline{T}$, is the density of forces with regard to the effective area $A_0 - A$.

Effective Stress

The damage variable is related to the usual stress vector, T, by

$$\overline{T} = T \frac{A_0}{A_0 - A}$$

or

$$\overline{T} = \frac{T}{1 - \frac{A}{A_0}} = \frac{T}{1 - w}$$

Which leads to the relation between the effective Cauchy stress tensor $\overline{\sigma}$ and the usual stress tensor σ by:

$$\overline{\sigma} = \frac{\sigma}{1 - w}$$
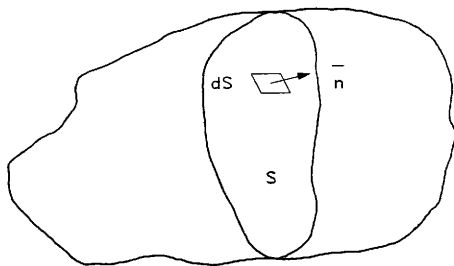
S = Section of the body
n̄ = Unit Normal vector defining
the small plane dS

Fig. 13. Damaged Element.

Stress–Strain Relation

Assuming, for simplicity, that the stress can be replaced by the effective stress, the one–dimensional stress–strain relations are

$$\epsilon^e = \frac{\sigma}{E} \qquad \text{in undamaged state}$$

$$\epsilon^e = \frac{\overline{\sigma}}{E} = \frac{\sigma}{(1-w)E} \qquad \text{in damaged state}$$

where ϵ^e is the elastic strain and E is Young's Modulus.

To fully develop a damage mechanics model, it is necessary to formulate state–type variables or memory–type variables, then define a thermodynamic potential or evolution law. From these preliminaries many models may be derived based on the choice of analytical expressions for the dissipative function. The scope of this study is to deal with the microplane model. In the microplane model a damage variable is not explicitly specified. Damage is accounted for through the microplane normal strains at points in a body. For a detailed look at damage mechanics models, the reader is referred to the references mentioned in this chapter and in the literature review.

DEVELOPMENT OF THE MICROPLANE MODEL

Three Dimensions

Hypotheses

1. Relation of ϵ_{ij} to e_n

The normal microstrain, e_n, which governs the progressive development of cracking in a concrete body, on a microplane at any orientation, is equal to the resolved component of the macroscopic strain tensor on the same plane, Fig. 14. As shown in Fig. 14, the solid lines between aggregates represent microplanes.

$$e_n = n_i n_j \epsilon_{ij} \qquad i, j = 1, 3 \qquad (1)$$

where e_n = the normal component of the strain on an arbitrary microplane.

In this hypothesis, the macroscopic strain tensor ϵ_{ij} corresponds to the relative displacements of the centroids of the aggregate particles. The normal component of ϵ_{ij}, e_n, corresponds to the deformation of the thin mortar layers between the aggregate particles, which are assumed to be rigid. Since the mortar deformation is assumed to be related to the aggregate particle displacements, ϵ_{ij} is assumed to be related to e_n.

Use of a kinematic restraint, such as $e_n = n_i n_j \epsilon_{ij}$, is advantageous because for any given value of strain, only one value of stress exists. The reverse is not true. Further, a static restraint, such as $\sigma_n = n_i n_j \sigma_{ij}$ was not assumed because the microstresses are far from uniform due to stress concentrations at the locations where the aggregate particles are closest together.

2. Normal Micro–stress

The stress relief due to all microcracks normal to $\overline{n}$ is characterized by assuming that the microstress σ_n on a microplane of any orientation is a function of e_n on
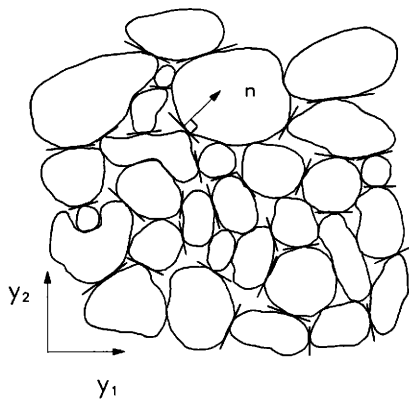
Fig. 14. Schematic Picture of Microstructure.

the same plane.

$$\sigma_n = F(e_n) \tag{2}$$

and

$$\frac{d\sigma_n}{de_n} = F'(e_n)$$

Here, no attempt is made to relate the shear stress on any microplane to the macroscopic strains. The shear stress on any such microplane is assumed to be zero, which is not to say that the macroscopic shear stresses in the body are zero. This assumption is reasonable if the crack opening tends to prevail over the crack slip, and the shear stiffness due to aggregate interlock is negligible. In a more rigorous effort, Bažant (1984) developed a theory to include shear stress on microplanes. Bažant's development of the microplane model follows.

Relation of σ_{ij} to σ_n

To develop the stress–strain relation, the principle of virtual work may be used. Consider an arbitrary point surrounded by a small sphere of radius r in a volume of material subjected to stresses, σ_{ij}, and strains, ϵ_{ij}. The virtual strain energy in the spherical volume or the work δW done by macroscopic stresses within the spherical volume is

$$\delta W = \int \int \int \sigma_{ij} \delta \epsilon_{ij} dV$$

Using the spherical coordinate system, Fig. 15, this integral can be expressed as

$$\delta W = \int_{\rho=0}^{r} \int_{\theta=0}^{2\pi} \int_{\phi=0}^{\pi} \sigma_{ij} \delta \epsilon_{ij} (\rho^2 sin\phi d\phi d\theta) d\rho$$

and reduces to

$$\delta W = \frac{4}{3} \pi r^3 \sigma_{ij} \delta \epsilon_{ij} \tag{3}$$
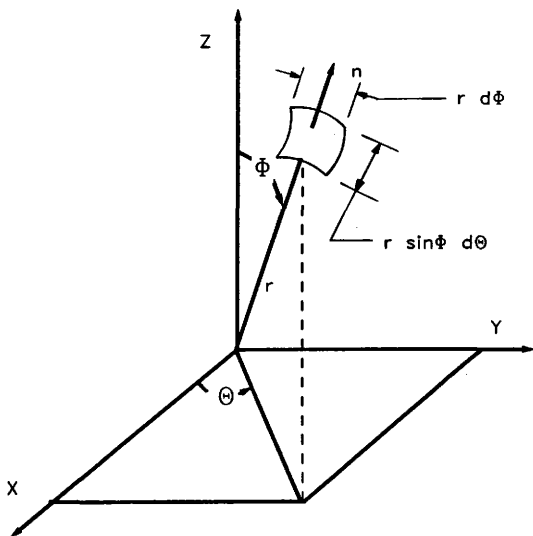
Fig. 15. Microplane in Spherical Coordinates.

The virtual work done by the stresses on the surface of the sphere is

$$\delta W = \int_{2S} \sigma_n(r\delta e_n)f(\overline{n})dS$$

where $2S$ = the surface area of the sphere, $dS = r^2 sin\phi d\theta d\phi$, $f(\overline{n})$ = the given normalized frequency distribution of microplanes of various orientations, characterizing the anisotropic properties of the material. For initially isotropic materials, $f(\overline{n}) \equiv 1$. Integrating over the surface S of the hemisphere and multiplying by 2 gives

$$\delta W = 2r \int_S \sigma_n \delta e_n dS \tag{4}$$

Substituting (1) and (2) into (4)

$$\delta W = 2r \int_{\theta=0}^{2\pi} \int_{\phi=0}^{\frac{\pi}{2}} F(e_n)\delta(n_i n_j \epsilon_{ij})(rd\phi)(r sin\phi)d\theta \tag{5}$$

Setting (3) equal to (5)

$$\delta W = \frac{4}{3}\pi r^3 \sigma_{ij}\delta\epsilon_{ij} = 2r^3 \int_{\theta=0}^{2\pi} \int_{\phi=0}^{\frac{\pi}{2}} F(e_n)n_i n_j \delta\epsilon_{ij} sin\phi d\phi d\theta \tag{6}$$

From hypothesis 1, (5) must hold for any microplane orientation. Cancelling $\delta\epsilon_{ij}$ and the constant, r^3, and simplifying,

$$\sigma_{ij} = \int_{\theta=0}^{2\pi} \int_{\phi=0}^{\frac{\pi}{2}} \frac{3}{2\pi}F(e_n)n_i n_j sin\phi d\phi d\theta \tag{7}$$

Differentiating $F(e_n)$ by the chain rule,

$$dF(e_n) = F'(e_n)de_n$$

substituting (1),

$$dF(e_n) = F'(e_n)n_k n_m d\epsilon_{km} \tag{8}$$

differentiating (7),

$$d\sigma_{ij} = \int_0^{2\pi} \int_0^{\frac{\pi}{2}} \frac{3}{2\pi} dF(e_n) n_i n_j sin\phi d\phi d\theta$$

and substituting (8), yields

$$d\sigma_{ij} = \int_0^{2\pi} \int_0^{\frac{\pi}{2}} \frac{3}{2\pi} F'(e_n) n_i n_k n_m sin\phi d\phi d\theta$$

Introducing

$$D_{ijkm}^c = \int_0^{2\pi} \int_0^{\frac{\pi}{2}} \frac{3}{2\pi} F'(e_n) a_{ijkm} sin\phi d\phi d\theta \qquad (9)$$

where $F'(e_n) = \frac{d\sigma_n}{de_n}$ and $a_{ijkm} = n_i n_j n_k n_m$, we have

$$d\sigma_{ij} = D_{ijkm}^c d\epsilon_{km} \qquad (10)$$

where D_{ijkm}^c is the tangent stiffness matrix of the microplane system.

Restriction on Poisson's Ratio

A restriction on Poisson's ratio is implied by hypothesis 1. In the microplane system, let the elastic Poisson's ratio be denoted as ν_n, and let the elastic Poisson's ratio of the body as a whole be denoted as ν_c. To show the restriction on ν_n consider uniaxial strain:

$$\epsilon_{33} \neq 0 \qquad \text{all other} \quad \epsilon_{ij} = 0$$

From Fig. 13,

$$n_1 = sin\phi cos\theta$$

$$n_2 = sin\phi sin\theta$$

$$n_3 = cos\phi$$

and from (1),

$$e_n = n_3^2 \epsilon_{33}$$

Assume for $\epsilon_{33} \ll 1; F(e_n) = E_n e_n$, where $E_n = F'(0) < \infty$. E_n is called the elastic modulus of the microplane.

Solving for σ_{33} using (7)

$$\sigma_{33} = \frac{3}{2\pi} \int_0^{2\pi} \int_0^{\frac{\pi}{2}} F(e_n) n_3 n_3 sin\phi d\phi d\theta \tag{11}$$

Substituting $e_n = n_3^2 \epsilon_{33}$ and $n_3 = cos\phi$ into (11)

$$\sigma_{33} = \frac{3}{2\pi} \int_0^{2\pi} \int_0^{\frac{\pi}{2}} E_n \epsilon_{33} cos^4\phi d\phi d\theta$$
$$= \frac{3}{5} E_n \epsilon_{33} \tag{12}$$

Solving for σ_{22}

$$\sigma_{22} = \frac{3}{2\pi} \int_0^{2\pi} \int_0^{\frac{\pi}{2}} E_n e_n n_2 n_2 sin\phi d\phi d\theta$$
$$= \frac{1}{5} E_n \epsilon_{33} \tag{13}$$

The ratio between the transverse and longitudinal stresses is, from (12) and (13),

$$\frac{\sigma_{22}}{\sigma_{33}} = \frac{\frac{2\pi}{15} E_n \epsilon_{33}}{\frac{2\pi}{5} E_n \epsilon_{33}} = \frac{1}{3} \tag{14}$$

Now recall Hooke's law,

$$\sigma_{ij} = \frac{E}{1+\nu} \left(\epsilon_{ij} + \frac{\nu}{1-2\nu} \epsilon_{kk} \delta_{ij} \right)$$

where E and ν are Young's modulus and Poisson's ratio, respectively, from which

$$\sigma_{22} = \frac{E\nu}{(1+\nu)(1-2\nu)} \epsilon_{33}$$

$$\sigma_{33} = \frac{E(1-\nu)}{(1+\nu)(1-2\nu)} \epsilon_{33}$$

and

$$\frac{\sigma_{22}}{\sigma_{33}} = \frac{\nu}{1-\nu} \qquad (15)$$

Solving for ν from (14) and (15),

$$\frac{\nu}{1-\nu} = \frac{1}{3}$$

$$\nu = \frac{1}{4}$$

Hence, the value of Poisson's ratio imposed by the microplane model is 0.25.

Correction of the Incremental Stiffness Matrix

A value of $\nu = 0.25$ is inapplicable for concrete, which has a Poisson ratio, ν_c, of 0.18. Hence, ν must be corrected. Bažant proposed to adjust ν by introducing an additional elastic strain ϵ_{ij}^a into the microplane model so that the total strain of the material is

$$\epsilon_{ij}{}^{tot} = \epsilon_{ij} + \epsilon_{ij}^a$$

The elastic compliance matrix is given by

$$C_{ijkm} = \frac{1-2\nu}{3E}\delta_{ij}\delta_{km} + \frac{1+\nu}{E}(\delta_{ik}\delta_{jm} - \frac{1}{3}\delta_{ij}\delta_{km}) \qquad (16)$$

Introduce the additional bulk and shear moduli, K^a and G^a, respectively:

$$K^a \geq K = \frac{E}{3(1-2\nu)} = \text{ initial bulk modulus}$$

$$G^a \geq G = \frac{E}{2(1+\nu)} = \text{ initial shear modulus}$$

Substituting K^a and G^a into (16), the compliances corresponding to the additional elastic strain are given by

$$C_{ijkm}^a = \frac{1}{9K^a}\delta_{ij}\delta_{km} + \frac{1}{2G^a}(\delta_{ik}\delta_{jm} - \frac{1}{3}\delta_{ij}\delta_{km}) \qquad (17)$$

Determination of K^a and G^a

According to Bažant, C_{ijkm}^a must be made as stiff as possible to maintain computer simulation stability. To do this, he suggests that either $1/G^a$ or $1/K^a$ must vanish. Further, Bažant claims that, in general, if $1/K^a > 0$ and $1/G^a = 0$, the Poisson ratio, ν, of the body as a whole is less than the Poisson ratio, ν_n, of the microplane system. If $1/K^a = 0$ and $1/G^a > 0$, then ν is greater than ν_n. Here, select $1/G^a = 0$ because $\nu_c = 0.18$ and $\nu_n = 0.25$. Setting $1/G^a = 0$ and writing (17) in matrix form :

$$
C^a = \begin{bmatrix}
1/(9K^a) & 1/(9K^a) & 1/(9K^a) & 0 & 0 & 0 \\
& 1/(9K^a) & 1/(9K^a) & 0 & 0 & 0 \\
& & 1/(9K^a) & 0 & 0 & 0 \\
& & & 0 & 0 & 0 \\
& & \text{sym} & & 0 & 0 \\
& & & & & 0
\end{bmatrix}
$$

An alternative approach is to use only the diagonal terms and omit the off diagonal terms this compliance matrix.

Incorporating the compliances due to the additional elastic strain, ϵ_{ij}, into Hooke's law and using Voigt notation :

$$
\begin{Bmatrix}
\epsilon_1 \\
\epsilon_2 \\
\epsilon_3 \\
\epsilon_4 \\
\epsilon_5 \\
\epsilon_6
\end{Bmatrix}
= \frac{1}{E}
\begin{bmatrix}
1 & -\nu & -\nu & 0 & 0 & 0 \\
& 1 & -\nu & 0 & 0 & 0 \\
& & 1 & 0 & 0 & 0 \\
& & & 2(1+\nu) & 0 & 0 \\
& \text{sym} & & & 2(1+\nu) & 0 \\
& & & & & 2(1+\nu)
\end{bmatrix}
\begin{Bmatrix}
\sigma_1 \\
\sigma_2 \\
\sigma_3 \\
\sigma_4 \\
\sigma_5 \\
\sigma_6
\end{Bmatrix}
$$

$$
+ \begin{bmatrix}
1/(9K^a) & 1/(9K^a) & 1/(9K^a) & 0 & 0 & 0 \\
& 1/(9K^a) & 1/(9K^a) & 0 & 0 & 0 \\
& & 1/(9K^a) & 0 & 0 & 0 \\
& & & 0 & 0 & 0 \\
& \text{sym} & & & 0 & 0 \\
& & & & & 0
\end{bmatrix}
\begin{Bmatrix}
\sigma_1 \\
\sigma_2 \\
\sigma_3 \\
\sigma_4 \\
\sigma_5 \\
\sigma_6
\end{Bmatrix} \quad (18)
$$

To determine K^a, consider a plane stress state in which

$$\sigma_1 \neq 0 \qquad \text{all other} \quad \sigma_i = 0$$

From (18),

$$\epsilon_1 = \frac{\sigma_1}{E} + \frac{\sigma_1}{9K^a} \tag{19}$$

$$\epsilon_2 = \frac{-\nu\sigma_1}{E} + \frac{\sigma_1}{9K^a} \tag{20}$$

All other $\epsilon_i = 0$. By definition,

$$\nu \equiv -\frac{\epsilon_2}{\epsilon_1} \tag{21}$$

Substituting (19) and (20) into (21);

$$\nu = \frac{\nu_n \sigma_1 / E_n - \sigma_1 / (9K^a)}{\sigma_1 / E_n + \sigma_1 / (9K^a)}$$

and solving for K^a,

$$\frac{\nu}{E_n}\sigma_1 + \frac{\nu}{9K^a}\sigma_1 = \frac{\nu_n}{E_n - \sigma_1/(9K^a)}\sigma_1$$

$$\frac{\sigma_1}{9K^a}(1 + \nu) = \frac{\sigma_1}{E_n}(\nu_n - \nu)$$

$$K^a = \left(\frac{1 + \nu}{\nu_n - \nu}\right)\frac{E_n}{9} \tag{22}$$

Equation (22) applies for $\nu \leq \nu_n$ and $G^a \to \infty$.

Incremental Stress–Strain Relation

The incremental stress–strain relation is given by

$$d\sigma_{ij} = D_{ijkm} \ d\epsilon_{km}$$

where

$$D_{ijkm} = \left[(D_{ijkm}^c)^{-1} + C_{ijkm}^a\right]^{-1}$$

D_{ijkm} = the adjusted tangent stiffness matrix.

D_{ijkm}^{e} = the tangent stiffness matrix.

C_{ijkm}^{a} = the compliance matrix corresponding to the additional elastic strain, ϵ_{ij}^{a}.

Microplane Constitutive Law

Since tensile strain softening is to be modelled, σ_n, as a function of e_n, must first rise to a maximum, and then gradually decline to zero. Bažant chose an exponential function to describe behavior in the strain softening region because σ_n approaches zero asymtotically on the declining branch of the curve. The smootheness of the function is computationally convenient, because its derivative is defined everywhere.

$$\text{For} \quad e_n > 0: \qquad \sigma_n = E_n e_n e^{-(ke_n^p)} \qquad (\text{If} \quad de_n \geq 0)$$

$$\text{For} \quad e_n \leq 0: \qquad \sigma_n = E_n e_n$$

where

$k = (1/\epsilon_0)^p$

ϵ_0 = value of strain at maximum uniaxial tensile stress.

p = Material constant which must be greater than or equal to unity in order for the slope and curvature to be continuous through the point $e_n = 0$.

Numerical Integration on the Surface of a Hemisphere

Numerical integration over the surface of a unit hemisphere may be used to evaluate the integral in (7). The numerical integration formula may be written in the form

$$D_{ijkm}^{c} \cong \sum_{\alpha=1}^{N} w_{\alpha} \left[a_{ijkm} F'(e_n) \right]_{\alpha} \tag{23}$$

where w_{α} = weighting factors.

$\alpha = 1, 2, ... N$ = Number of numerical integration points on the unit hemispherical surface, defined by the unit vectors, $\overline{n}_{\alpha}$. The significance of (23) lies in the need for

an efficient integration scheme. Since there are 6 independent incremental stiffnesses in (7), the numerical integration must be carried out 6 times for each point of the material where the stiffness is needed. In a finite element program, the numerical integration must be carried out for all integration points of each finite element, and for all iterations. Thus, an efficient numerical integration scheme is of great value.

A number of Gauss type numerical formulas by Albrecht and Collatz, Finden, Sobolev, McLaren, and Stroud are given in Stroud's book (1971). In an effort to optimize the numerical integrataion, Bažant and Oh (1983B) devised some new formulas, based on Taylor series expansions. These formulas rely on computer operations to find the weights and point locations on the surface of the sphere for which the error is minimized. For the case of plane stresses or plane strains, Bažant and Oh proposed a 21-point formula of degree 9, which gives an error of about 3%.

Two Dimensions

In the case of concrete subjected to plane stresses or plane strains, only the microplanes normal to the reference plane are considered, Fig. 16 (a). This simplification may cause the model to be too stiff in certain situations characterized by concrete damage along the oblique microplanes, with respect to the reference plane. However, the simplification is advantageous because it decreases the number of direction cosines for each microplane from 3 to 2.

<div align="center">

Hypotheses

</div>

1. Relation of ϵ_{ij} to e_n

This hypothesis is identical to hypothesis 1 in the 3-dimensional case except i and j are summed to 2 instead of 3.

2. Normal Micro-stress
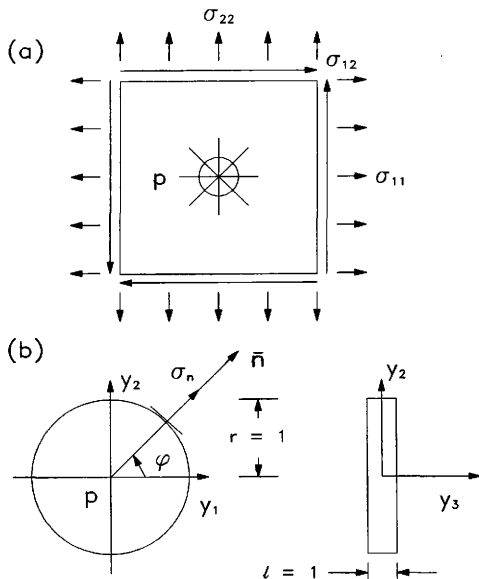
Fig. 16. (a) Idealization of the Material as a Microplane System and (b) Reference Volume for Writing the Equilibrium Conditions Between the Two Stress Systems, σ_{ij} and σ_n.

For 2-dimensional cases, Gambarova and Floris (1986) proposed

$$\sigma_n = F(e_n)e_n$$

where

$$\frac{d\sigma_n}{de_n} = F'(e_n)e_n + F(e_n)$$

Relation of σ_{ij} to σ_n

To develop the relation between σ_{ij} and σ_n, consider a cylinder of unit radius and unit length centered at a point P in a body, Fig. 16 (b). Now apply the principle of virtual work by considering all microplanes of arbitrary orientations passing through P (Gambarova and Floris 1986). The virtual work done at P by the macroscopic stresses is

$$\delta W = \int \int \int \sigma_{ij}\delta\epsilon_{ij}dV$$

where dV = the volume of the cylinder. The expression reduces to

$$\delta W = \sigma_{ij}\delta\epsilon_{ij}(\pi r^2 l)$$

For unit radius and length:

$$\delta W = \pi\sigma_{ij}\delta\epsilon_{ij} \tag{24}$$

Now consider the virtual work done on the surface of the cylinder by the microstresses:

$$\delta W = 2\int_0^\pi \sigma_n\delta e_n d\phi \tag{25}$$

Equating (24) and (25),

$$\pi\sigma_{ij}\delta\epsilon_{ij} = 2\int_0^\pi \sigma_n\delta e_n d\phi \tag{26}$$

Substituting hypothesis 1 into (26);

$$\pi\sigma_{ij}\delta\epsilon_{ij} = 2\int_0^\pi \sigma_n\delta(n_in_j\epsilon_{ij})d\phi$$

$$= 2\int_0^\pi \sigma_n n_in_j\delta\epsilon_{ij}d\phi \tag{27}$$

Now $\delta\epsilon_{ij}$ is a family of virtual strains and does not vary with ϕ. Taking $\delta\epsilon_{ij}$ outside the integral in (27) and dividing both sides of the equation by π:

$$\sigma_{ij}\delta\epsilon_{ij} = \frac{2}{\pi}\delta\epsilon_{ij}\int_0^\pi \sigma_n n_in_j d\phi$$

Cancelling $\delta\epsilon_{ij}$ from both sides;

$$\sigma_{ij} = \frac{2}{\pi}\int_0^\pi \sigma_n n_in_j d\phi \tag{28}$$

Differentiating (28) gives

$$d\sigma_{ij} = \frac{2}{\pi}\int_0^\pi d\sigma_n n_in_j d\phi \tag{29}$$

Recalling Hypothesis 2;

$$\sigma_n = F(e_n)e_n$$

$$d\sigma_n = \left(\frac{\partial F}{\partial e_n}e_n + F(e_n)\frac{\partial e_n}{\partial e_n}\right)de_n$$

$$= \left(\frac{dF}{de_n} + F(e_n)\right)de_n \tag{30}$$

Substituting (30) into (29);

$$d\sigma_{ij} = \frac{2}{\pi}\int_0^\pi \left(\frac{dF}{de_n} + F(e_n)\right)de_n n_in_j d\phi \tag{31}$$

Differentiating hypothesis 1;

$$de_n = n_kn_m d\epsilon_{km} \tag{32}$$

Substituting (32) into (31);

$$d\sigma_{ij} = \frac{2}{\pi} \int_0^\pi \left(\frac{dF}{de_n} e_n + F(e_n) \right) n_i n_j (n_k n_m d\epsilon_{km}) d\phi \tag{33}$$

Define

$$a_{ijkm} \equiv n_i n_j n_k n_m \tag{34}$$

and substituting (34) into (33);

$$d\sigma_{ij} = \frac{2}{\pi} \int_0^\pi \left(\frac{dF}{de_n} e_n + F(e_n) \right) a_{ijkm} d\epsilon_{km} d\phi$$
$$= \left[\frac{2}{\pi} \int_0^\pi a_{ijkm} \left(\frac{dF}{de_n} e_n + F(e_n) \right) d\phi \right] d\epsilon_{km} \tag{35}$$

where i, j, k, m = 1,2

Letting

$$D_{ijkm} = \frac{2}{\pi} \int_0^\pi a_{ijkm} \left(\frac{dF}{de_n} e_n + F(e_n) \right) \tag{36}$$

and substituting (36) into (35);

$$d\sigma_{ij} = D_{ijkm} d\epsilon_{km} \tag{37}$$

where D_{ijkm} = the tangent stiffness of the microplane system.

Restriction on Poisson's Ratio

As in the 3–dimensional case a restriction on Poisson's ratio is implied by hypothesis 1. To show the restriction on ν_n, consider a case which has only small values of strain, for which the tangent stiffness in (37) must reduce to the elastic stiffness matrix. For e_n tending to zero,

$$\sigma_n = E_n e_n$$

This implies that

$$F(e_n) = \frac{\sigma_n}{e_n} \tag{38}$$

Substituting (38) into (35);

$$d\sigma_{ij} = \left[\frac{2}{\pi}\int_0^\pi a_{ijkm}\left(\frac{dF}{de_n}0 + E_n\right)d\phi\right]d\epsilon_{km} \quad \text{(for } e_n \to 0)$$

$$= \left[\frac{2E_n}{\pi}\int_0^\pi n_i n_j n_k n_m d\phi\right]d\epsilon_{km}$$

Solving for $d\sigma_{11}$;

$$d\sigma_{11} = \left[\frac{2E_n}{\pi}\int_0^\pi n_1 n_1 n_k n_m d\phi\right]d\epsilon_{km}$$

$$= \frac{3E_n}{4}\left[d\epsilon_{11} + \frac{1}{3}d\epsilon_{22}\right] \tag{39}$$

Solving for $d\sigma_{22}$;

$$d\sigma_{22} = \frac{2E_n}{\pi}\int_0^\pi n_2 n_2 n_k n_m d\phi d\epsilon_{km}$$

$$= \frac{3E_n}{4}\left[\frac{1}{3}d\epsilon_{11} + d\epsilon_{22}\right] \tag{40}$$

Solving for $d\sigma_{12}$;

$$d\sigma_{12} = \frac{2E_n}{\pi}\int_0^\pi n_1 n_2 n_k n_m d\phi d\epsilon_{km}$$

$$= \frac{1}{2}E_n d\epsilon_{12} \tag{41}$$

Now consider uniaxial strain:

$$\epsilon_{11} \neq 0 \qquad \text{all other} \quad \epsilon_{ij} = 0$$

For this arbitrary example, (39) and (40) reduce to

$$d\sigma_{11} = \frac{3}{4}E_n d\epsilon_{11}$$

and

$$d\sigma_{22} = \frac{1}{4}E_n d\epsilon_{11}$$

Then

$$\frac{d\sigma_{22}}{d\sigma_{11}} = \frac{(1/4)E_n d\epsilon_{11}}{(3/4)E_n d\epsilon_{11}} = \frac{1}{3}$$

Since the principle of superposition holds for small stresses and stains, the incremental relations become total relations;

$$\frac{\sigma_{22}}{\sigma_{11}} = \frac{1}{3}$$

For plane stresses;

$$\frac{\sigma_{22}}{\sigma_{11}} = \frac{(E/1 - \nu^2)(d\epsilon_{22} + \nu d\epsilon_{11})}{(E/1 - \nu^2)(d\epsilon_{11} + \nu d\epsilon_{22})} = \frac{\nu d\epsilon_{11}}{d\epsilon_{11}} = \nu$$

Thus, ν is restricted to be

$$\nu = \frac{1}{3} \quad \text{(plane stress problems)}$$

For plane strains:

$$\frac{\sigma_{22}}{\sigma_{11}} = \frac{\frac{E(1-\nu)}{(1+\nu)(1-2\nu)}(d\epsilon_{22} + \frac{\nu}{1-\nu})d\epsilon_{11}}{\frac{E(1-\nu)}{(1+\nu)(1-2\nu)}(d\epsilon_{11} + \frac{\nu}{1-\nu})d\epsilon_{22}} = \frac{\nu}{1 - \nu}$$

Thus, ν is restricted to be

$$\nu = \frac{1}{4} \quad \text{(plane strain problems)}$$

E_n as a Function of E_c

To simplify implementation of the microplane model into an existing finite element analysis program, it is necessary to relate the microplane modulus E_n to the elastic material modulus E_c.

For plane stresses,

$$d\sigma_{11} = \frac{E}{1 - \nu^2}(d\epsilon_{11} + \nu d\epsilon_{22}) \tag{42}$$

$$d\sigma_{22} = \frac{E}{1 - \nu^2}(d\epsilon_{22} + \nu d\epsilon_{11}) \tag{43}$$

$$d\sigma_{12} = \frac{E}{(1 + \nu)}d\epsilon_{12} \tag{44}$$

Equating (39) and (42), (40) and (43), (41) and (44), respectively;

$$\frac{3E_n}{4}\left[d\epsilon_{11} + \frac{1}{3}d\epsilon_{22}\right] = \frac{E}{1-\nu^2}(d\epsilon_{11} + \nu d\epsilon_{22})$$

$$\frac{3E_n}{4}\left[\frac{1}{3}d\epsilon_{11} + d\epsilon_{22}\right] = \frac{E}{1-\nu^2}(d\epsilon_{22} + \nu d\epsilon_{11})$$

$$\frac{1}{2}E_n d\epsilon_{12} = \frac{E}{1+\nu}d\epsilon_{12}$$

To express E_n as a function of E_c and Poisson's ratio, ν_c, consider a uniaxial state of stress. Previously, it was shown that ν is restricted to be $\frac{1}{3}$ for plane stresses. Substituting $\nu = \frac{1}{3}$ into any of the above three equations, and solving for E_n :

$$E_n = 1.5E \qquad \text{for plane stresses}$$

For plane strains,

$$d\sigma_{11} = \frac{E(1-\nu)}{(1+\nu)(1-2\nu)}(d\epsilon_{11} + \frac{\nu}{1-\nu}d\epsilon_{22}) \qquad (45)$$

$$d\sigma_{22} = \frac{E(1-\nu)}{(1+\nu)(1-2\nu)}(d\epsilon_{22} + \frac{\nu}{1-\nu}d\epsilon_{11}) \qquad (46)$$

$$d\sigma_{12} = \frac{E}{1+\nu}d\epsilon_{12} \qquad (47)$$

Equating (39) and (45), (40) and (46), (41) and (47), respectively;

$$\frac{3E_n}{4}\left[d\epsilon_{11} + \frac{1}{3}d\epsilon_{22}\right] = \frac{E(1-\nu)}{(1+\nu)(1-2\nu)}(d\epsilon_{11} + \frac{\nu}{1-\nu}d\epsilon_{22})$$

$$\frac{3E_n}{4}\left[\frac{1}{3}d\epsilon_{11} + d\epsilon_{22}\right] = \frac{E(1-\nu)}{(1+\nu)(1-2\nu)}(d\epsilon_{22} + \frac{\nu}{1-\nu}d\epsilon_{11})$$

$$\frac{1}{2}E_n d\epsilon_{12} = \frac{E}{1+\nu}d\epsilon_{12}$$

Previously, it was shown that ν is restricted to be $\frac{1}{4}$ for plane strains. Substituting $\nu = \frac{1}{4}$ into any of the above three equations :

$$E_n = 1.6E \qquad \text{For plane strains}$$

Correction of Poisson's Ratio

As in the 3-dimensional case, an additional compliance matrix will be used to correct the initial or elastic Poisson ratio. The additional strains ϵ_{ij}^a and stresses σ_{ij}^a are purely volumetric and hydrostatic, respectively. An adjustment of the microplane modulus is also necessary. As a result, in uniaxial tension, the effective Poisson's ratio was observed to first increase to a peak and then decrease asymptotically. The effect is an increase in volume of the body, followed by a decrease in volume of the body, which is opposite of what happens for uniaxial compression.

Adjustment of Modulus E_n

Plane Stresses :

Recall Hooke's law, with additional strains, ϵ_{ij}^a;

$$\epsilon_{ij} = \left(\frac{1+\nu}{E} \sigma_{ij} - \frac{\nu}{E} \sigma_{kk} \delta_{ij} \right) + \epsilon_{ij}^a$$

In a given plane stress problem from (18),

$$\epsilon_{11} = \left[\frac{1+\nu}{E_n} \sigma_{11} - \frac{\nu_n}{E_n}(\sigma_{11} + \sigma_{22}) \right] + (1/(9K^{a^*}))(\sigma_{11} + \sigma_{22})$$

Substituting $K^{a^*} = (1+\nu_c)/(\nu_n - \nu_c)E_n/9$,

$$\epsilon_{11} = \frac{1}{E_n} \left(\frac{1+\nu_n}{1+\nu_c} \right) (\sigma_{11} - \nu\sigma_{22})$$

Letting $E_n^* =$ the adjusted microplane modulus,

$$\epsilon_{11} = \frac{1}{E_n^*} \left(\frac{1+\nu_n}{1+\nu_c} \right) (\sigma_{11} - \nu\sigma_{22})$$

For convenience, drop the *. Introduce the microplane modulus as

$$E_n = 1.5 E_c \left(\frac{1+\nu_n}{1+\nu_c} \right)$$

which has been adjusted to comply with the correction of the Poisson's ratio.

Plane strains :

Recall Hooke's law with additional stresses, σ_{ij}^a,

$$\sigma_{ij} = \frac{E_n}{1 + \nu}\left[\epsilon_{ij} + \frac{\nu_n}{1 - 2\nu_n}\epsilon_{kk}\delta_{ij}\right] + \sigma_{ij}^a$$

Using the inverted form of (18) in a given plane strain problem,

$$\sigma_{11} = \frac{E_n}{1 + \nu}\left[\epsilon_{11} + \frac{\nu_n}{1 - 2\nu_n}(\epsilon_{11} + \epsilon_{22})\delta_{ij}\right] + K^{a^{**}}(\epsilon_{11} + \epsilon_{22})$$

Substituting $K^{a^{**}} = E_n(\nu_c - \nu_n)\Big/(1 - 2\nu_c)(1 + \nu_c)(1 - 2\nu_n)$

$$\sigma_{11} = \frac{E_n}{(1 + \nu_n)}\frac{(1 - \nu_c)}{(1 - 2\nu_c)}(\epsilon_{11} + \frac{\nu_c}{1 - \nu_c}\epsilon_{22})$$

Letting E_n^{**} = the adjusted microplane modulus,

$$\sigma_{11} = E_n^{**}(\epsilon_{11} + \frac{\nu_c}{1 - \nu_c}\epsilon_{22})$$

which coincides with Hooke's law on the condition that

$$E_n^{**} = E_n\frac{1 + \nu_n}{1 + \nu_c}$$

For convenience, drop the **. Introduce the microplane modulus as

$$E_n = 1.6E_c\frac{1 + \nu_n}{1 + \nu_c}$$

which has been adjusted to comply with the correction of the Poisson's ratio.

Correction of the Incremental Stiffness Matrix

For plane stresses, the additional compliances are

$$C^a = \begin{bmatrix} 1/(9K^{a^*}) & 1/(9K^{a^*}) & 0 \\ & 1/(9K^{a^*}) & 0 \\ & \text{sym} & 0 \end{bmatrix}$$

where

$$K^{a^*} = \left(\frac{1 + \nu_c}{\nu_n - \nu_c} \right) \frac{E_c}{9}$$

For plane strains, the additional stiffnesses are

$$D^a = \begin{bmatrix} K^{a^{**}} & K^{a^{**}} & 0 \\ & K^{a^{**}} & 0 \\ \text{sym} & & 0 \end{bmatrix}$$

where

$$K^{a^{**}} = \frac{E_c(\nu_c - \nu_n)}{(1 + \nu_c)(1 - 2\nu_c)(1 - 2\nu_n)}$$

Incremental Stress–Strain Relation

The incremental stress–strain relation in 2–dimensions is identical to that of 3–dimensions except i, j, k, and m are summed to 2 instead of 3.

Microplane Constitutive Law

(Bažant and Oh 1983A)

1. Tension

$$\sigma_n = E_n e_n exp[-(a_1 e_n + b_1 e_n^2)] \tag{48}$$

$$\frac{d\sigma_n}{de_n} = E_n exp(-(a_1 e_n + b_1 e_n^2)) \times (1 - e_n(a_1 + b_1 e_n)) \tag{49}$$

which reduces to a linear–elastic relation for small strain values, Fig. 17. The constants a_1 and b_1 are

$$a_1 = (1/\epsilon_0)[2ln(E_n \epsilon_0 / \sigma_0) - 1]$$

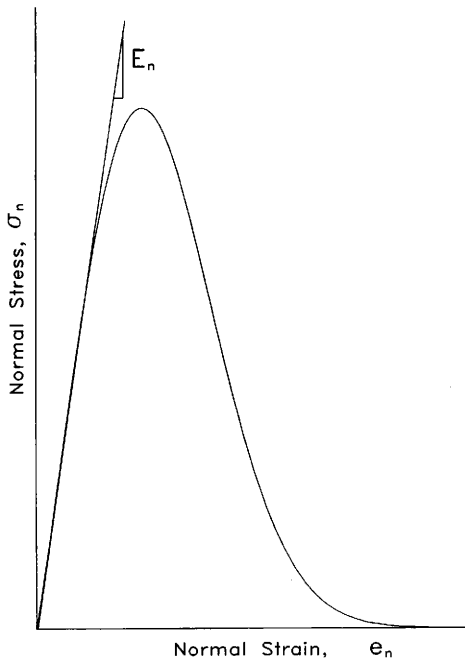$$b_1 = (1/\epsilon_0^2)[1 - ln(E_n \epsilon_\theta / \sigma_0)]$$

Fig. 17. Constitutive Law for a
Microplane in Tension.

where

$$\epsilon_0 = (1.67 f'_c + 92.3) \times 10^{-6}$$

$$\sigma_0 = k f_{ct} \qquad (f'_c, f_{ct} = MPa, 6.895 MPa = 1000 psi)$$

$$k = [2.57 + (12.4 f'_c + 0.0214 f'^2_c) \times 10^{-3}]/2$$

$$f_{ct} = 0.35 (f'_c)^{2/3}$$

2. Compression

$$\sigma_n = \frac{2}{\pi} |\sigma_\infty| arctan(\omega e_n) \qquad (50)$$

$$\frac{d\sigma_n}{de_n} = \frac{2}{\pi} |\sigma_\infty| \omega/(1 + \omega^2 e_n^2) \qquad (51)$$

where

$$\omega = \pi E_n/(2|\sigma_\infty|)$$

$$|\sigma_\infty| = f'_c \left[0.59(1 + 2.06 exp(-200\epsilon^*) \right]$$

$$\leq f'_c \left[1.45 + 0.0089(f'_c - 18.84) \right]$$

$\epsilon^* = 0$ for compression. The constitutive laws for concrete in compression are shown in Fig. 18, where σ_∞ is a function of f'_c, and E_n is a funtion of E_c.

3. Unloading after Tension

$$\sigma_n = -a_2 + \beta \ arctan[(E'_n/\beta)(e_n - b_2)] \qquad (52)$$

$$\frac{d\sigma_n}{de_n} = E'_n/(1 + (E'n(e_n - b_2)/\beta)^2)$$

where

$$a_2 = -(\sigma_\infty + \beta\pi/2)$$

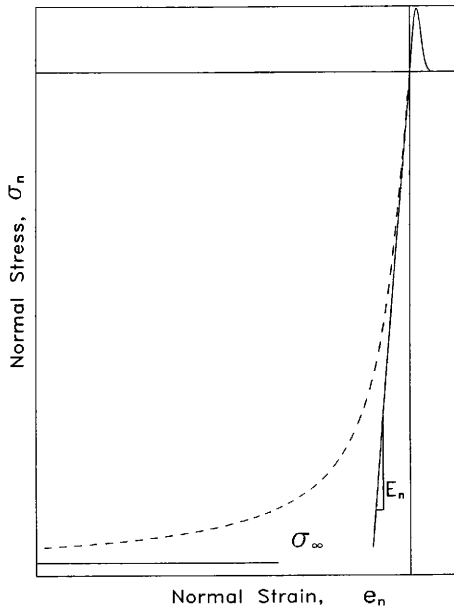$$b_2 = \epsilon^* - (\beta/E'_n)tan[(\sigma^* + a_2)/\beta]$$

Fig. 18. Constitutive Law for a
Microplane in Compression.

$$\beta = \frac{1.05}{\pi}|\sigma_\infty|(1 + 1.38exp(-400\epsilon^*))$$

$$\beta \leq 2\frac{|\sigma_\infty|}{\pi}$$

$$E_n' = E_n a[1 + b \quad exp(-c(\epsilon^* - 2.5\epsilon_0)^{0.25}] \leq E_n$$

$$a = 0.06(f_c'/31)^2$$

$$b = 16.7(31/f_c')^2 - 1$$

$$c = 10(31/f_c')^{0.25}$$

A family of unloading curves are shown if Fig. 19. The curves show the dependence of compressive strength, σ_∞, on the amount of tensile damage the body has previously experienced.

4. Unloading after Compression

$$\sigma_n = \sigma^{**}exp\left[\frac{E_n''}{\sigma^{**}}(e_n - \epsilon^{**})\right] \tag{53}$$

$$\frac{d\sigma_n}{de_n} = E_n''exp(E_n(e_n - \epsilon^{**})/\sigma^{**}) \tag{54}$$

where E_n'' is the tangent modulus at the point of unloading and may be taken as

$$E_n'' = \sigma^{**}/\epsilon^{**} \quad \text{or} \quad E_n'' = E_n$$

A family of reloading curves is shown in Fig. 20, which shows the locations of $\epsilon^*, \sigma^*, \epsilon^{**}, \sigma^{**}$. As shown in Fig. 20, the amount of hysteresis the body undergoes during reloading greatly depends on the point of reloading.

Numerical Integration over a Unit-Cylinder

The numerical integration formula used to evaluate (36) is

$$D_{ijkm} = \frac{2}{\pi}\Delta\Phi\sum_{\alpha=1}^{N}(a_{ijkm}\frac{d\sigma_n}{de_n})_\alpha \tag{55}$$
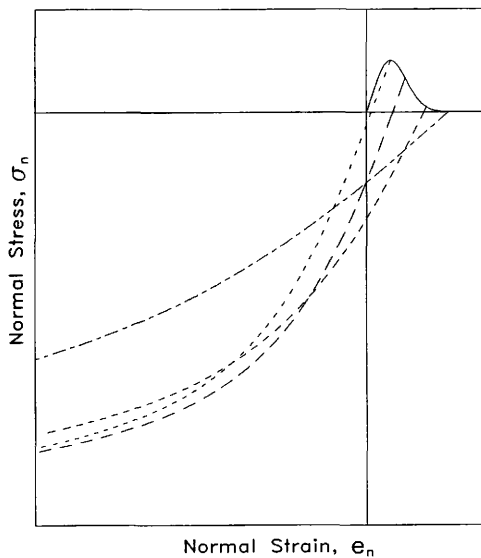
Fig. 19. Constitutive Laws for a Microplane
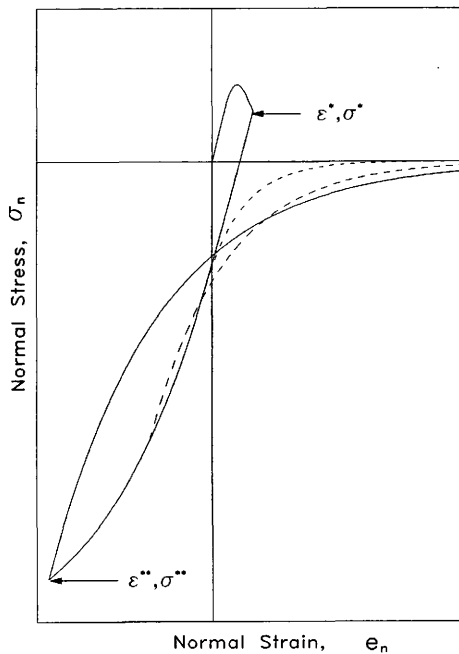Subjected to Unloading in Tension.

Fig. 20. Constitutive Laws for a Microplane Unloading after Compression.

in which the integration is carried out over a regular half-polygon, having N sides. Gambarova and Floris (1986) investigated the response of concrete under plane stresses for different numbers and orientations of planes for the same load histories, and concluded that relatively few planes are needed to obtain a description which is independent of the number and orientation of the microplanes. Specifically, they found that 6, 12, or 24 planes give reasonable results. In this investigation, 12 planes are used and oriented as shown in Fig. 21.

Cracking Criterion

In order to quantify the damage in a body, a cracking pattern may be drawn, based on a stress or a strain criterion. The cracking criterion used here is based on strain. Once the maximum principal strain reaches the value of strain, ϵ_0, on the uniaxial stress–strain curve, which corresponds to the peak stress, σ_0, then a crack is assumed to exist normal to the direction of maximum principal strain. This is done external to the microplane model and is used only to quantify the damage in the body. A strain criterion, rather than a stress criterion, was used here because it is believed that strain more realistically defines the point at which a specimen undergoes major microcacking than does stress. This belief is supported by the work of Kaplan (1963), who found that strains at cracking and near ultimate failure were independent of the types of aggregate and water to cement ratios used in the experiment, while stresses were not. It is also supported by other, more recent, works in the literature (Tasuji, Slate, and Nilson 1978; Carino and Slate 1976; Slate and Meyers 1968; Newman 1968).
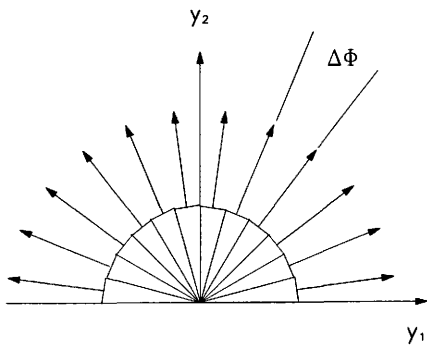
y_1, y_2 = Global Coordinate axes.

Fig. 21. Orientation of the 12 Microplanes.

NUMERICAL RESULTS

Uniaxial and Biaxial Tension

To investigate uniaxial and biaxial tension behavior of concrete, one four–noded, plane stress quadrilateral element was loaded with two point loads as shown in Fig. 22. Various material constants were considered from Table 3, which gives ϵ_0, σ_0, E_c, E_n, and σ_0/ϵ_0 for values of the compressive strength f_c' ranging from 3000 to 6000 psi. The table was constructed using the equations given by Gambarova and Floris (1986). It should be noted that ϵ_0 and σ_0 are microplane properties, instead of macroscopic properties. As expected, Fig. 23 shows an increase in tensile strength as compressive strength increases. Also, with increasing compressive strength, concrete becomes more brittle, which agrees with the experimental results of Evans and Marathe (1968) and Hughes and Chapman (1966).

Shown in Figs. 24–27. are microplane and macroscopic stress–strain curves for the four datasets shown in Fig. 23. The microplane datasets, generated directly from (48), show a higher strength and a more brittle behavior than the macroscopic datasets. The difference is due to the way the macroscopic stresses are determined in a nonlinear finite element analysis using the microplane model. First, the tangent stiffnesses, or incremental stiffnesses, are approximated using a summation of the products of the derivatives and the associated direction cosines for each microplane, equation (55). Then, since the incremental strains are known, the incremental stresses can be determined, from which the total stresses can be updated. Hence, it is the slope of the curve of the normal stress vs normal strain, not the value of normal stress, for each microplane which is used to determine the macroscopic behavior of the body. Inherently, this process causes the input curve, or microplane stress–strain curve, to differ from the output curve, or macroscopic stress–strain

+ = Integration Point
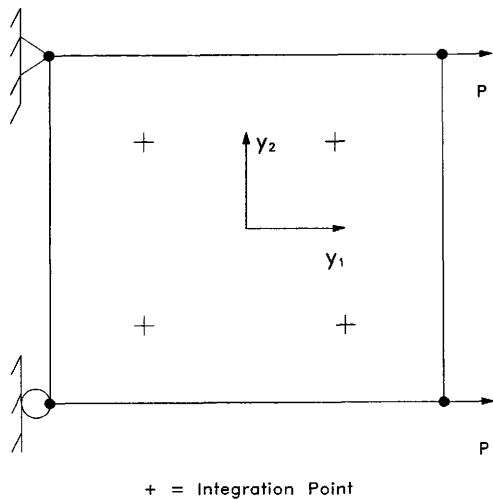
Fig. 22. Four—Noded Quadrilateral Element
Under Uniaxial Tension.
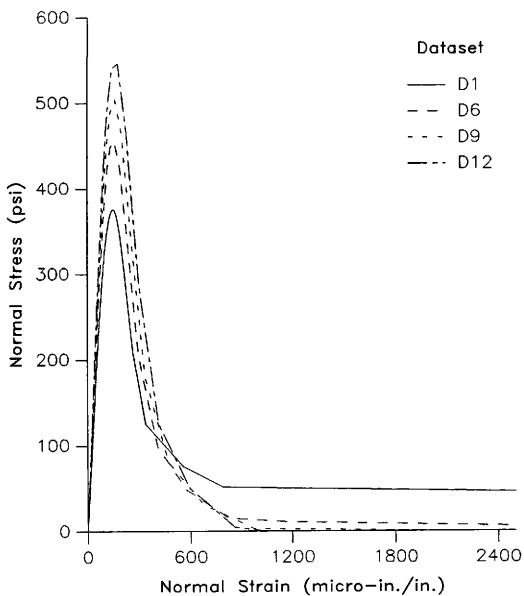
Fig. 23. Response of Plain Concrete to Uniaxial Tension.
(1 psi = 6.895 kPa)
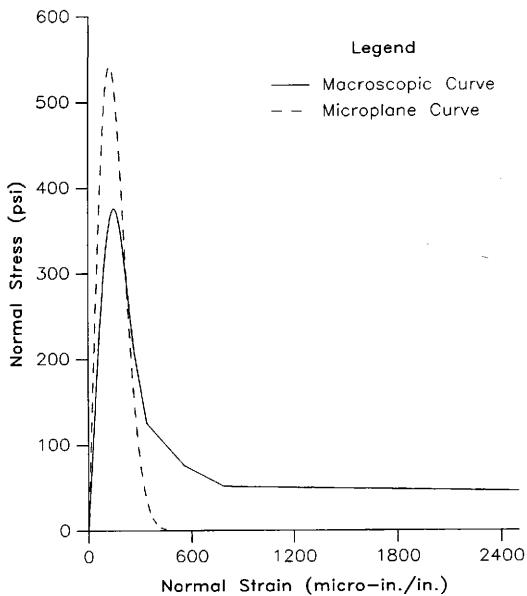
Fig. 24. Response of Plain Concrete to
Uniaxial Tension for dataset D1.
(1 psi = 6.895 kPa)

Fig. 25. Response of Plain Concrete to
Uniaxial Tension for dataset D6.
(1 psi = 6.895 kPa)

Fig. 26. Response of Plain Concrete to
Uniaxial Tension for dataset D9.
(1 psi = 6.895 kPa)

Fig. 27. Response of Plain Concrete to
Uniaxial Tension for dataset D12.
(1 psi = 6.895 kPa)

Table 3. Concrete Material Properties.

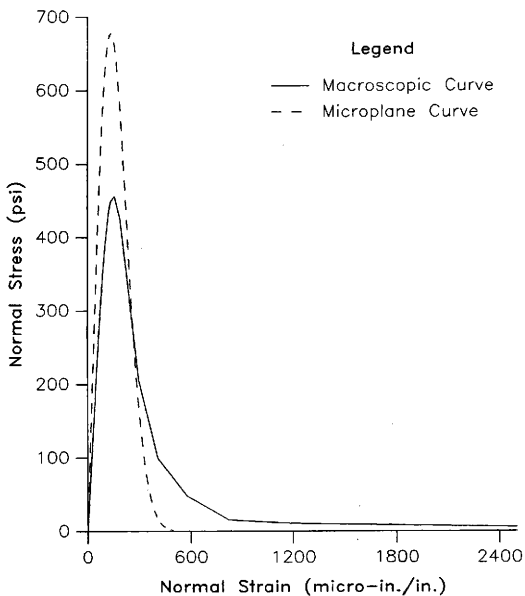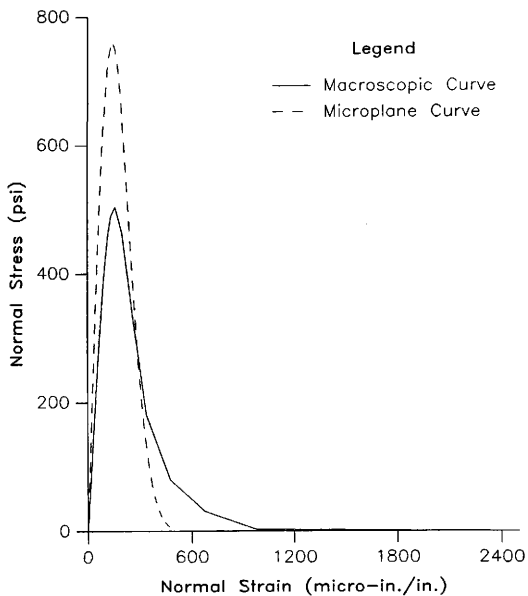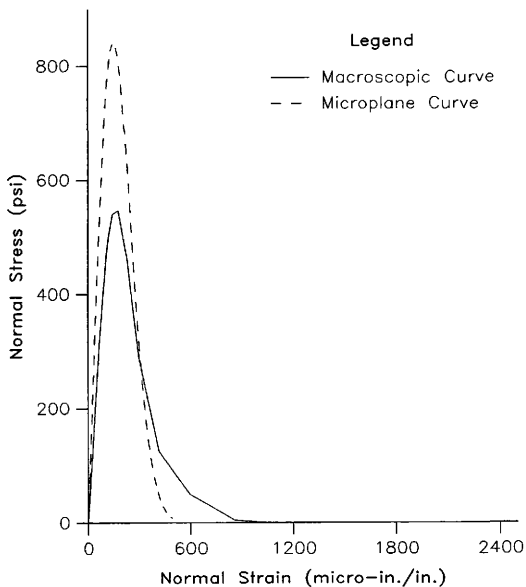| Dataset (1)	f'_c (psi) (2)	ϵ_0 (micro-in./in.) (3)	σ_0 (psi) (4)	E_c (psi) (5)	E_n (psi) (6)	σ_0/ϵ_0 (psi) (7)
D1	3000	127	542	3.32E+06	5.63E+06	4.27E+06
D2	3200	129	570	3.43E+06	5.81E+06	4.41E+06
D3	3400	131	597	3.54E+06	5.99E+06	4.54E+06
D4	3600	134	624	3.64E+06	6.17E+06	4.67E+06
D5	3800	136	651	3.74E+06	6.33E+06	4.79E+06
D6	4000	138	678	3.83E+06	6.50E+06	4.90E+06
D7	4200	141	705	3.93E+06	6.66E+06	5.02E+06
D8	4400	143	732	4.02E+06	6.82E+06	5.12E+06
D9	4600	145	759	4.11E+06	6.97E+06	5.23E+06
D10	4800	148	786	4.20E+06	7.12E+06	5.33E+06
D11	5000	150	813	4.29E+06	7.27E+06	5.42E+06
D12	5200	152	840	4.37E+06	7.41E+06	5.52E+06
D13	5400	155	866	4.46E+06	7.55E+06	5.61E+06
D14	5600	157	893	4.54E+06	7.69E+06	5.70E+06
D15	5800	159	920	4.62E+06	7.83E+06	5.78E+06
D16	6000	161	947	4.70E+06	7.96E+06	5.87E+06

curve.

To evaluate the accuracy the microplane model for uniaxial and biaxial tension, the experimental results of Tasuji, Slate, and Nilson (1978) were used. The researchers subjected concrete plates, 5 x 5 x 1/2 in., to biaxial stresses. A maximum loading rate of 140 psi/min. was used, and the specimens were loaded so that the

stress ratios were constant throughout the test.

The concrete used consisted of type III portland cement. It had a water-to-cement ratio of 0.6 and a fine aggregate-to-cement ratio of 1.88, both by weight. The maximum aggregate size was 0.5 in. The age of the concrete was 2 weeks. Deformations in the plane of the specimens were measured with 4 in. electrical strain gages, and deformations normal to the plane of the specimens were measured with a Fonotonic Sensor. The tensile elastic modulus, Poisson's ratio, and maximum strength were 3.03 E06 psi, 0.16, and 440 psi, respectively. Taking $f'_c = 4000$ psi, the calculated microplane properties, ϵ_0 and σ_0, are 138 micro-in./in. and 678 psi, respectively.

The results of three of their tests are shown in Figs. 28-30. The results indicate that as the amount of applied transverse stress increases, the longitudinal maximum strength increases. This does not mean that the strength of the material increases, but only that the material can carry more load in biaxial tension than in uniaxial tension. Comparison between the experimental results and the microplane model shows good agreement. In previous work, Donida, Floris, and Gambarova (1987) fitted the data for two of the three cases considerd here and found identical results with the microplane model.

Pure Shear after Uniaxial Tension

To investigate pure shear, one four-noded, plane stress quadrilateral element was used as in the case of uniaxial tension. The same properties were used as in uniaxial tension for the four example runs. Specimens were first subjected to uniaxial tensile stresses equal to 0, 30%, 60%, or 90% of the maximum uniaxial, macroscopic tensile strength. Then, with the tensile stress held constant, shear stress increments were added.
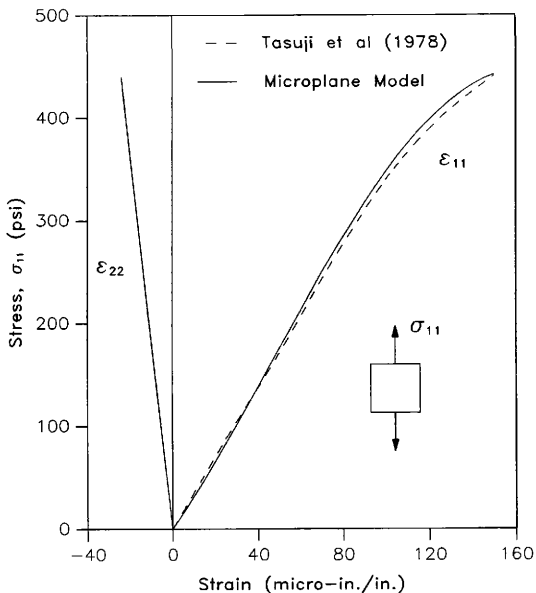
Fig. 28. Stress–Strain Relationship for Plain Concrete Under Uniaxial Tension.
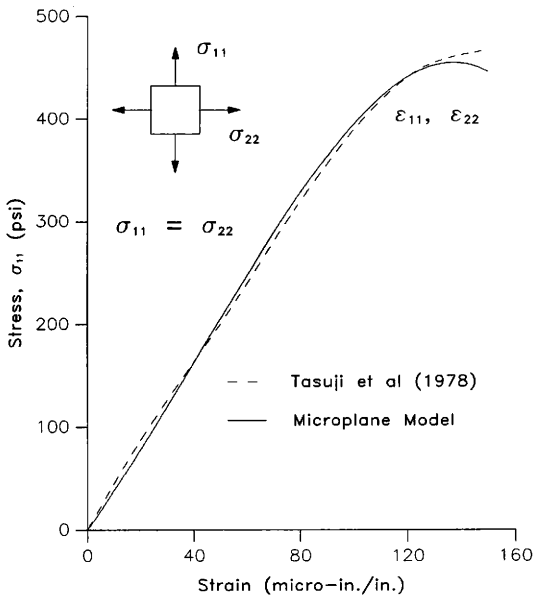(1 psi = 6.895 kPa)

Fig. 29. Stress–Strain Relationship for Plain Concrete Under Biaxial Tension ($\sigma_{11} = \sigma_{22}$).
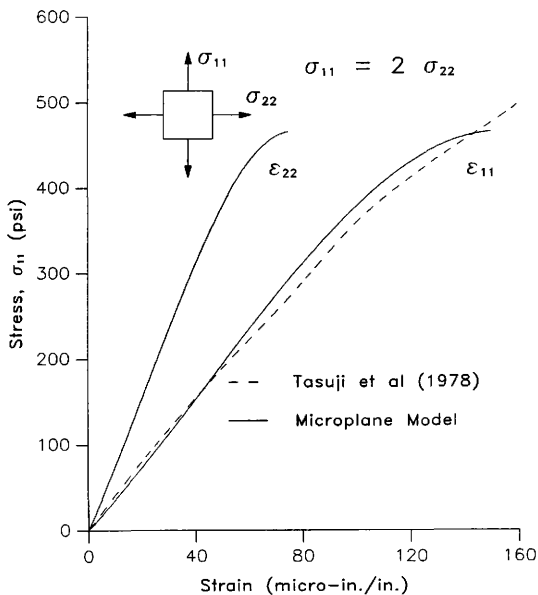(1 psi = 6.895 kPa)

Fig. 30. Stress—Strain Relationship for Plain Concrete Under Biaxial Tension ($\sigma_{11} = 2\ \sigma_{22}$). (1 psi = 6.895 kPa)

Results of the analysis are shown in Figs. 31–38. The curves in Figs. 32, 34, 36, and 38 show large variance in response to pure shear for different degrees of tensile damage between 0 and 900 micro–in./in. However, Figs. 31, 33, 35, and 37 show that the datasets converge to approximately the same curve at high values of shear strain. The reason for these results lies in the behavior of the individual microplanes. In uniaxial tension, the microplanes more nearly normal to the direction of applied load experience tensile strains. The microplanes more nearly parallel to the direction of the load experience compressive strains. Because of these compressive strains, some of the microplanes show compressive stress–strain relations. This is not to say that the macroscopic transverse stress is nonzero for uniaxial tension, but only that that some of the microplane constitutive relations are compressive in nature. When the shear load is applied, some of the microplanes unload from compression while some others unload from tension. The magnitude of macroscopic tensile loading dictates how far in tension or compression each microplane will go prior to application of pure shear. Hence, at lower values of shear strain, the curves are different. However, once large values of normal strain on each microplane are reached, the normal micro–stresses have reached their respective asymptotic compressive or tensile values. At this point, the derivatives of the equations for normal stress are approximately zero, and the peak value of shear stress has been reached. The result is that the same ultimate shear strength will be reached regardless of the tensile stress applied if the applied tensile stress is below the maximum tensile stress.

Shear–Panel

The panel analyzed is shown in Fig. 39. It has a height of 7 in., a height of 15 in., and a span of 30 in. A vertical concentrated load P is applied at midspan. The

Fig. 31. Response of Plain Concrete to Pure Shear after Uniaxial Tension for dataset D1. (1 psi = 6.895 kPa)

Fig. 32. Expanded Plot of Plain Concrete Response to Pure Shear after Uniaxial Tension for dataset D1. (1 psi = 6.895 kPa)
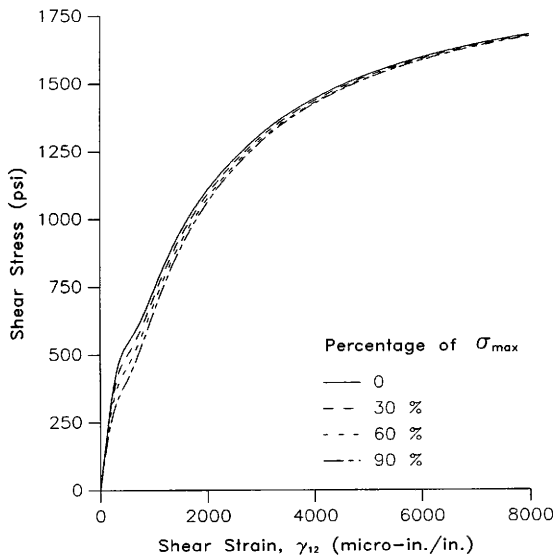
Fig. 33. Response of Plain Concrete to Pure Shear after Uniaxial Tension for dataset D6. (1 psi = 6.895 kPa)
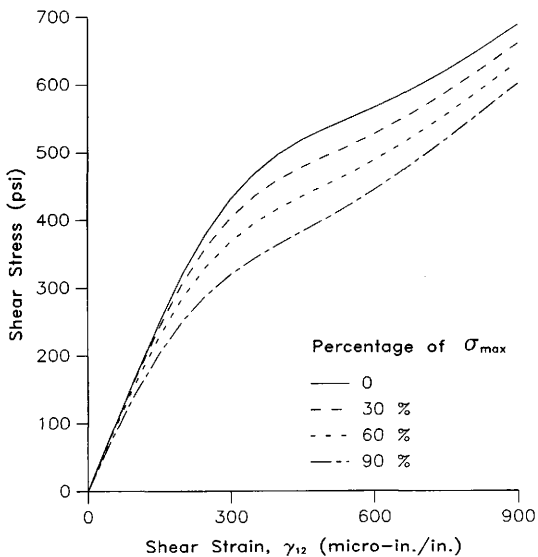
Fig. 34. Expanded Plot of Plain Concrete Response to Pure Shear after Uniaxial Tension for dataset D6. (1 psi = 6.895 kPa)

Fig. 35. Response of Plain Concrete to Pure Shear after Uniaxial Tension for dataset D9. (1 psi = 6.895 kPa)

Fig. 36. Expanded Plot of Plain Concrete Response to Pure Shear after Uniaxial Tension for dataset D9. (1 psi = 6.895 kPa)
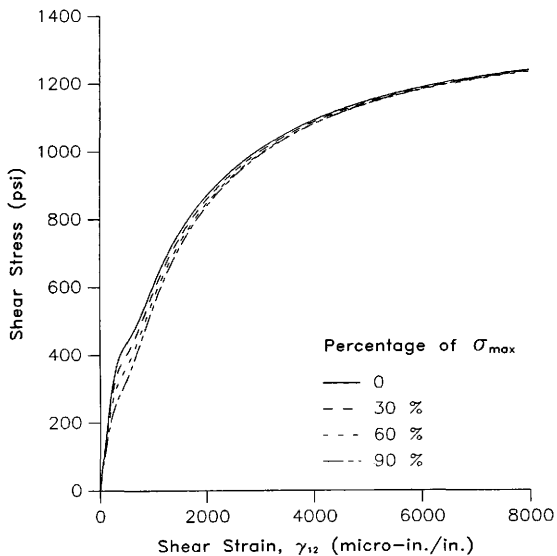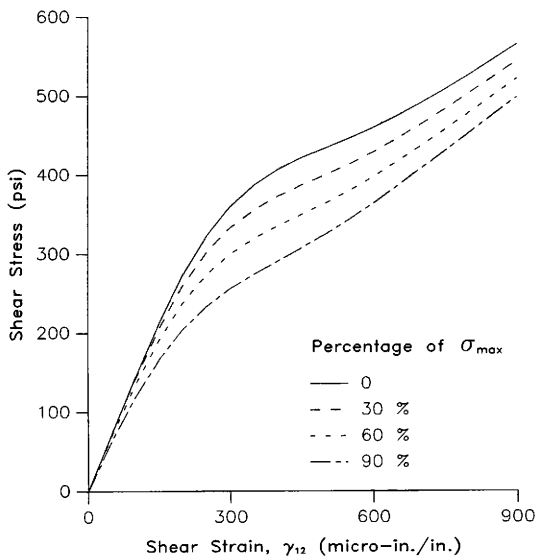
Fig. 37. Response of Plain Concrete to Pure Shear after Uniaxial Tension for dataset D12.
(1 psi = 6.895 kPa)
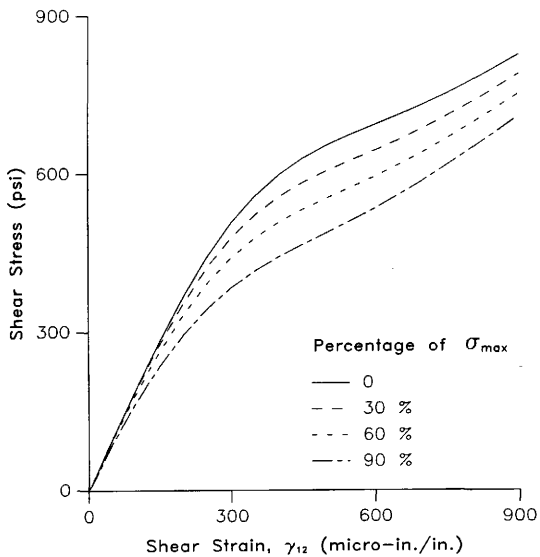
Fig. 38. Expanded Plot of Plain Concrete Response to Pure Shear after Uniaxial Tension for dataset D12. (1 psi = 6.895 kPa)
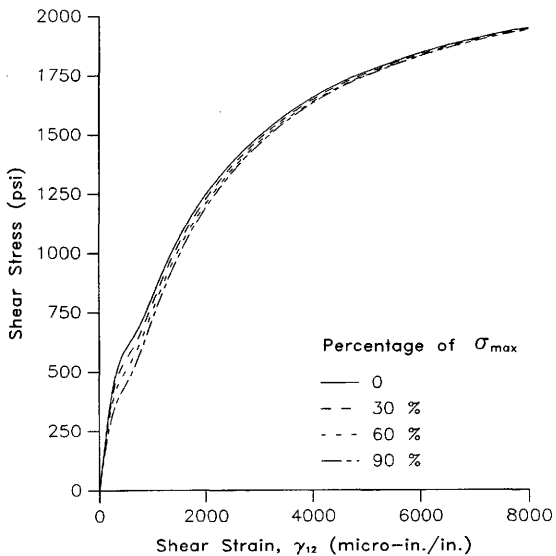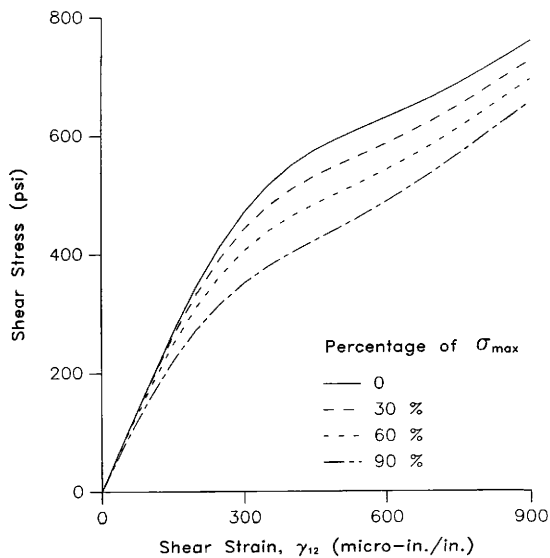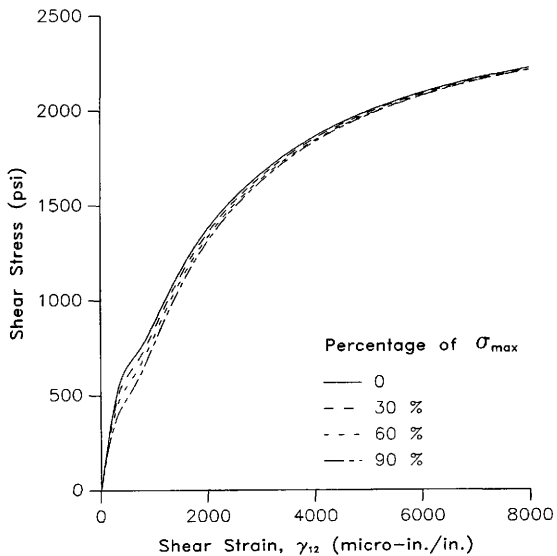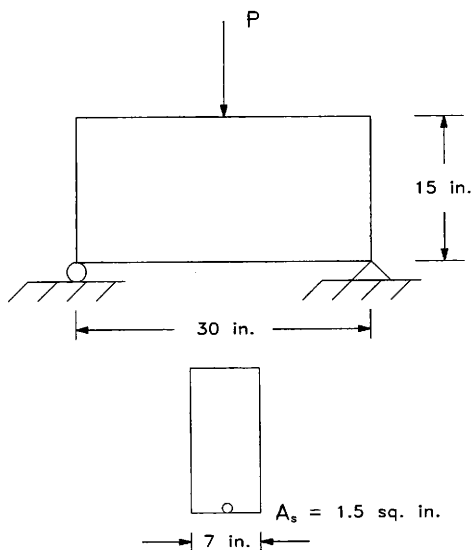
Fig. 39. Shear—Panel Example.
(1 in. = 25.4 mm)

steel reinforcement has the cross–sectional area, $A_s = 1.5$ sq. in. and is modeled as being at the bottom of the beam. The ratio of reinforcing steel to cross-sectional area of concrete is $\rho = 0.014$. No shear reinforcement is present. The properties of the concrete are Young's modulus, $E_c = 3000$ ksi, Poisson's ratio, $\nu_c = 0.2$, and tensile strength, $f_t = 400$ psi. The properties of the reinforcing steel are Young's modulus, $E_s = 29,000$ ksi, Poisson's ratio, $\nu_s = 0.3$, and yield stress, $f_y = 60$ ksi.

Previously, Bažant and Cedolin (1980) studied the same beam. They used a mesh of constant strain triangles with 72 degrees of freedom. The concrete was assumed to be linearly elastic but, upon cracking, the shear modulus was reduced to 40% of its original value. These material assumptions were intended to crudely model aggregate interlock and avoid nonlinear behavior in compression. A strength criterion was used to determine when cracking initiates at any point in the beam. The steel reinforcement was modeled by bar elements connected to the bottom row of elements.

In the present study, the existing nonlinear finite element code ABAQUS, version 4.5, was used. The mesh was constructed of eight–noded quadrilateral elements. Material behavior was modeled using the microplane model with the assumption that any material point behaves orthotropically after cracking. The steel reinforcement was smeared into the bottom row of elements.

Shown in fig. 40 is the response of the beam using the model by Bažant and Cedolin (1980) and the microplane model. The difference between the two models is in the degradation of the material stiffness. Bažant and Cedolin assumed linear elastic moduli and a reduced shear modulus after cracking. In the microplane model, degradation of the stiffnesses are inherently built into the model through the individual microplane behavior. Despite the differences in the two models,
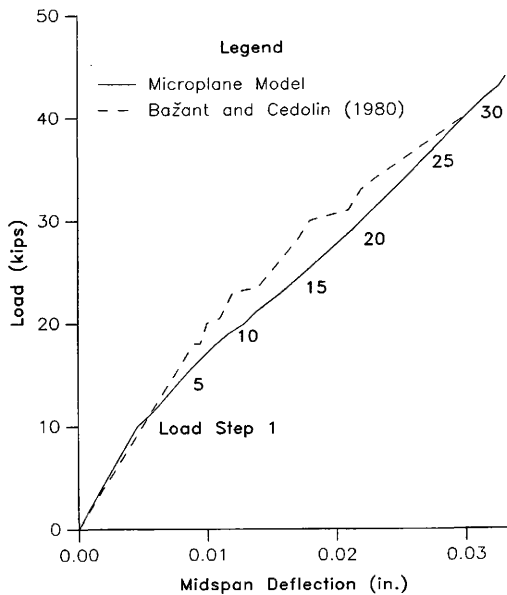
Fig. 40. Response of Shear–Panel to Concentrated Load.
(1 ksi = 6.895 MPa, 1 in. = 25.4 mm)

good agreement between them is observed.

Progressive fracture in the beam is tracked as shown in Fig. 41. The cracking pattern is typical of a short, deep beam. Shear cracks appear first at the end of the beam and are inclined at approximately 45 degrees. Flexural cracks also appear, starting at the tensile fibers at midspan, and advancing up the section of the beam and outward towards the end of the beam. The numbers on Fig. 41 indicate the load step at which each integration point cracked and are also shown on the load vs. midspan deflection curve, Fig. 40.

Problems of this type have been a point of controversy between researchers Darwin and Dodds (1982) and Bažant and Cedolin (1982). Much of their discord is in bridging the two parts of an extensive analysis of concrete structures. These two portions are crack initiation and crack propagation. Crack initiation is generally governed by a stress or a strain criterion. Crack propagation may be modeled using fracture mechanics. Recent research (Gustaffasson and Hillerborg 1988; Bažant 1987; Evans and Marathe 1968; Kaplan 1961) shows a trend toward the use of an energy criterion for crack propagation. The energy criterion may be based on a characteristic length of the body and tensile strength of the material.

The choice of whether to include fracture mechanics in the analysis depends on the problem to be studied. For problems dominated by propagation of individual cracks, such as dams, reactor vessels, bridge girders, and ocean structures, fracture mechanics should be included in the study. However, for problems in which overall, macroscopic behavior, such as general crack patterns and load–deflection reponses, are needed, a simple stress or strain criterion should be adequate (Darwin and Dodds 1982).
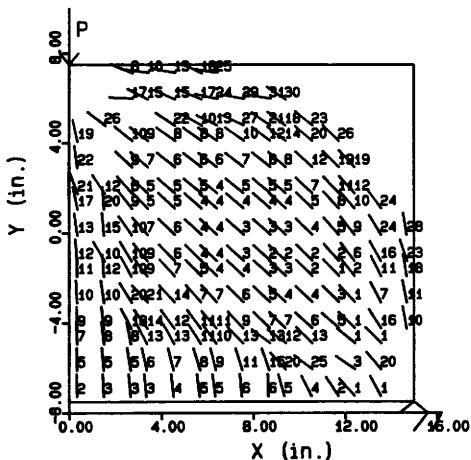
Fig. 41. Cracking Pattern of Concrete Shear—Panel.
(1 in. = 25.4 mm)

Bending of a One-Way Slab

The slab analyzed is shown in Fig. 42. It has a width of 18 in., a height of 1.5 in., and a span of 30 in. Two uniformly distributed vertical line loads P are applied across the slab width and are symmetrically placed about the middle line of the slab, 6 in. from either simple end support. Each steel reinforcing bar has a diameter of 3/16 in. The bars are spaced at 2.57 in. The ratio of reinforcing steel to cross-sectional area of concrete is $\rho = 0.0071$. The properties of the concrete are Young's modulus, $E_c = 4.2E06$, Poisson's ratio, $\nu_c = 0.18$, and compressive strength, $f'_c = 4580$ psi. The properties of the reinforcing steel are Young's modulus, $E_s = 29,000$ ksi, Poisson's ratio, $\nu_s = 0.3$, and yield stress, $f_y = 32$ ksi.

The concrete has a maximum aggregate size of 1/8 in., a water-to-cement ratio of 0.65 by weight, and an aggregate-to-cement ratio of 4.5 by weight. The aggregate is composed of 85% coarse aggregate and 15% sand.

In the nonlinear finite element analysis, two-noded beam elements with cubic interpolation functions were used. It is assumed that plane sections remain plane and no shear deformations exist. Two noded beam elements of lower order which follow the Bernoulli beam bending assumptions were not used, because they are not available in ABAQUS. Each cubic beam element contains three interpolation points along its span and nine section points at each integration point. One material constitutive relation is required at each section point, that being the relation between the stress and strain components normal to the plane of the beam's cross-section. The load was applied using two steps, the first going to 0.4 kips using automatic load incrementation control and the second going to the ultimate load using the Riks method. The loading was broken into two steps because the load-deflection response is essentially linear up to about 0.4 kips, after which highly
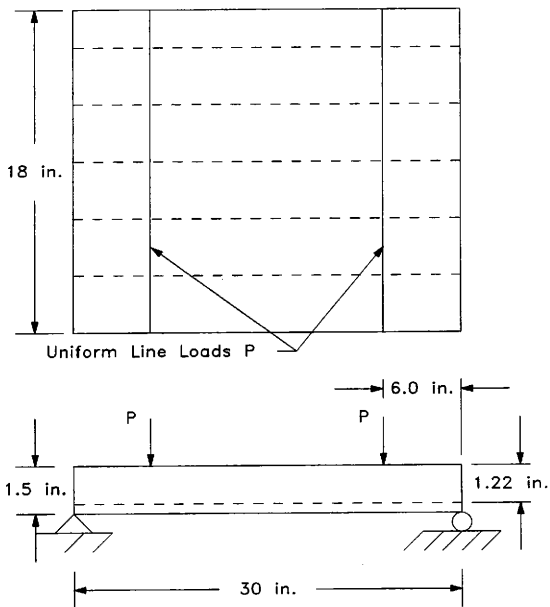
Fig. 42. One—Way Reinforced Concrete Slab
(Jain and Kennedy 1974).
(1 in. = 25.4 mm)

nonlinear behavior prevails. In the first step, load increments were controlled internally by ABAQUS to a total load of 0.4 kips. In the second step, a special feature called the Riks method (Crisfield 1981; Ramm 1981; Riks 1979) was used to model the collapse of the slab. The Riks method is a numerical algorithm used to model post–peak reponse of structures. More specifically, it may be used as a solution procedure to overcome limit points or collapse loads where there may exist a large decrease in load. Example applications are buckling of beams, large deflection analysis of shells, and, as shown here, collapse of reinforced concrete members.

The slab was first analyzed using the values of E_c and ν_c given above and with values of $\sigma_0 = 786$ psi and $\epsilon_0 = 148$ micro–in./in., from Table 3. Figure 43 shows convergence of the results to an ultimate load of about 0.660 kips. Also, the slope of the load–deflection curve very closely models the experimental data by Jain and Kennedy (1974). However, the calculated, empirical, values of σ_0 and ϵ_0 were observed to lead to a 50% underestimation of the ultimate load P of the slab, Fig. 43. It is thought that the underestimation of the ultimate load is due to a lack of tension stiffening in the model. In a cracked reinforced concrete flexural member such as the slab, the intact concrete between each pair of adjacent tensile cracks assists the tensile steel in carrying the internal tensile force, and therefore contributes to the overall bending stiffness of the member. Here, tension stiffening is defined as the amount of stiffness contributed to the steel by the concrete after cracking has occurred.

To account for tension stiffening, several approaches have been proposed. Jofriet and McNiece (1971) modeled tension stiffening through an empirically developed effective moment of inertia of the cracked slab section. Similiar work was done by Bell and Elms (1971). Gilbert and Warner (1978), Lin and Scordelis
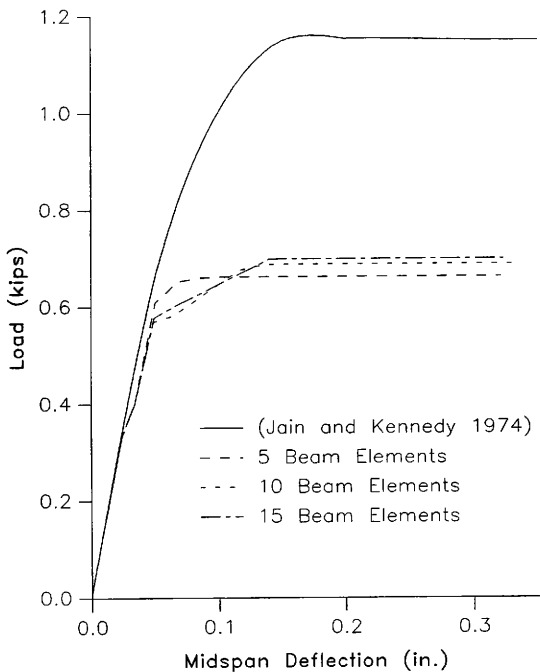
Fig. 43. Slab Response without Tension Stiffening.
(1 psi = 6.895 kPa, 1 in. = 25.4 mm)

(1975), Hand, Pecknold, and Schnobrick (1973), Scanlon (1971), and Wanchoo and May (1975) used a layered finite element approach to the problem in which they specified appropriate stress–strain relations for concrete and steel to represent the behavior of the various layers at different stages of loading. In the layered element approach, unloading curves are specified to model the tension stiffening effect. The same approach is used here because the microplane model inherently contains an unloading, or strain softening, portion of the uniaxial stress–strain curve.

The equations given by Gambarova and Floris (1985) model plain concrete quite accurately, as was shown earlier. However, to model tension stiffening, it is proposed to increase σ_0 and ϵ_0. At present, no analytical way of choosing the exact values of σ_0 and ϵ_0, which accurately model tension stiffening, are known. A trial and error approach was used to model the Jain and Kennedy slab response. When the values of σ_0 and ϵ_0 were increased to 1320 psi and 193 micro-in./in., respectively, the results closely model the test data, Fig. 44. The mesh used in this latter analysis consisted of 5 two-noded beam elements. Also shown in Fig. 44 is the analysis of the slab with no reinforcing steel. This analysis was done to show the effect of reinforcing steel on the ultimate load of the slab. In this case, the finite element analysis shows that the slab with reinforcing steel is about 7% stronger than the slab without steel reinforcement.
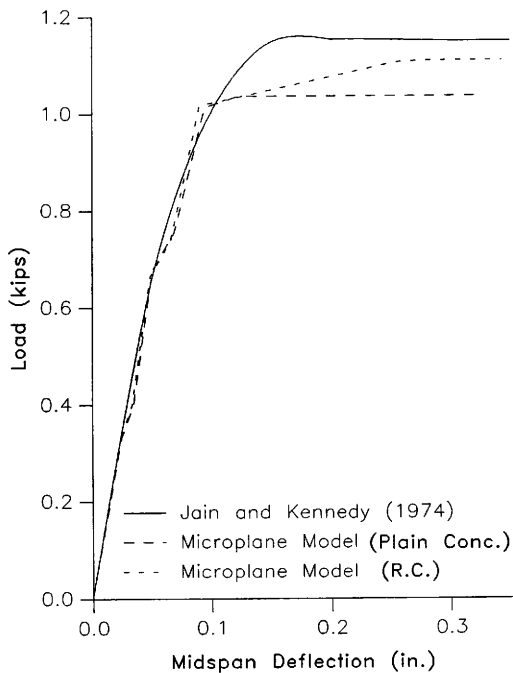
Fig. 44. Slab Response with Tension Stiffening.
(1 psi = 6.895 kPa, 1 in. = 25.4 mm)

CONCLUSIONS

Numerical Aspects

Four of the most important topics in a nonlinear finite element analysis of a concrete structure are element type, grid refinement, the constitutive model, and the load history. First, an appropriate element type and integration order must be chosen, depending on the problem. Examples of the importance of the element type and integration order were observed throughout this study. One such example is the uniaxial tension, biaxial tension, and pure shear cases shown earlier, where a four-noded, plane stress quadrilateral element with four integration points was adequate to obtain an accurate solution. However, in the beam-shear example, numerical instabilities were observed using the same element. Specifically, a convergent solution was not obtained using the four-noded quadrilateral element. An eight-noded, plane stress quadrilateral element with nine integration points gave a convergent solution.

Another example which shows the importance of the element on the results is the one-way slab example. Neither four-noded or eight-noded plane stress quadrilateral elements gave convergent solutions. Instead, both types of elements experienced numerical instabilities which caused divergent solutions. Beam elements with cubic interpolation functions gave reasonably accurate solutions compared to the experimental data. Thus, care must be taken in selecting the appropriate element type.

A second important numerical aspect is grid refinement. In order to assure that a convergent solution has been reached, at least two runs must be made. In the one-way slab response, three meshes were used to show convergence.

A problem with mesh convergence that was not investigated here is strain

localization, defined as the physical phenomenon in which a crack localizes into a thin band of material. This phenomenon is especially important if one wishes to investigate propagation of a single crack through a body. Bažant and Cedolin (1983) cited the example of a reinforced concrete panel in which a four–fold decrease in the element size caused the load for further crack band extension to drop by one–half. To eliminate the problem of crack propagation dependency on mesh size, crack band extensions based on energy criterions have been proposed (Bažant and Cedolin 1983). Strain localization was not studied here because attention was focused on gaining an understanding about the microplane model and obtaining macroscopic, overall results such as load–deflection curves and general crack patterns. In studies of structures such as dams, nuclear containment structures, and offshore structures, in which the problem may be dominated by propagation of a single crack, strain localization should be an integral part of the study.

A third important numerical aspect is the constitutive model to be used in the analysis. The choice of the constitutive model depends to a large extent on two things. First, the problem to be studied is an important guideline for choosing the constitutive model. If the problem is dominated by tensile stresses and strains, the microplane model studied here may be adequate. If the problem involves large compressive stresses and strains, the microplane model studied here is inadequate because it does not model compressive strain softening. It should be noted that in very recent work, Bažant, Pan, and Pijaudier–Cabot (1987) incorporated compressive strain softening into the microplane model. Furthermore, the model is not capable of modeling cyclic behavior of structures. Secondly, the computer dictates to a lesser extent the constitutive model. Here, double precision mode which carries about 16 significant digits, was used in ABAQUS. If the computations

are done in single precision mode, then significant errors can be expected in larger problems due to the great number of computations done during the analysis. In addition, storage of variables can be a problem. For every integration point in every element, 48 history–dependent variables are stored. These variables are the values of the microplane normal stress from the previous load increment, flags which identify an initial state of tension or compression on a microplane, and microplane strains and stresses corresponding to unloading from tension or compression. Four storage spaces are needed for each of the 12 microplanes at any integration point.

A fourth important aspect is the load history. Specifically, whether the loading is proportional or non–proportional can significantly affect the results. Proportional or radial loading is defined here as loading which causes the load path in stress space to originate at the origin and move outward from the origin along a straight line. In such a case,

$$\sigma_{11}/\sigma_{11}^Y = \sigma_{22}/\sigma_{22}^Y = \sigma_{12}/\sigma_{12}^Y$$

where σ_{11}^Y, σ_{22}^Y, and σ_{12}^Y are values of σ_{11}, σ_{22}, and σ_{12} at their yield strengths, respectively. Gambarova and Floris (1986) showed in their analysis of compression and torsion of hollow cylinders that the difference in ultimate strength can be significant depending on whether the loading is proportional or sequential, Figs. 45 and 46. These results agree with experimental results by Fouré (Gambarova and Floris 1986). The reason for the difference is in the behavior of each microplane. In the proportional load situation, the microplanes are always subjected to tension or compression, with no unloading. In the sequential load situation, some of the microplanes are in compression and some are in tension when macroscopic compression is applied. When torsional loading is applied, some microplanes unload from previous compression, and others unload from previous tension. From the

results shown in Figs. 45 and 46, it appears that the microplane model can model problems in which principal axes rotate due to non-proportional loading.

In addition to these four topics, the problem of numerical instability due to strain softening must be considered. Here, it became apparent that the Riks method is needed to overcome inherent numerical instablities caused by a strain softening material. Specifically, the examples studied here experienced numerical instabilities without the Riks method. Use of the Riks method allowed strain softening to take place without numerical instabilities.

The Microplane Model

In the results section, the microplane model was shown to accurately model uniaxial and biaxial tension. Further, the model gave results close to those obtained by Bažant and Cedolin (1980) for a beam dominated by shear stresses. In addition, it gave a convergent solution to bending of a one–way slab dominated by flexural stresses. However, more research must be done before the model studied here can be used with great confidence. First, the analytical results of the tension–shear stress test should be compared with experimental data. Second, tension stiffening should be researched in detail. This research may include tests on two reinforced beams. The first specimen should have undeformed reinforcing bars lubricated to prevent bond between concrete and steel, and the second should have reinforcing bars which allow steel–concrete bond. Hopefully, information would be gained about the interaction between the reinforcing steel and the concrete before and after cracking.

Several limitations of the microplane model are apparent. First, the model is limited to problems dominated by tensile stresses and strains. One way of solving this problem has been discussed by Bažant, Pan, and Pijauder–Cabot (1987),
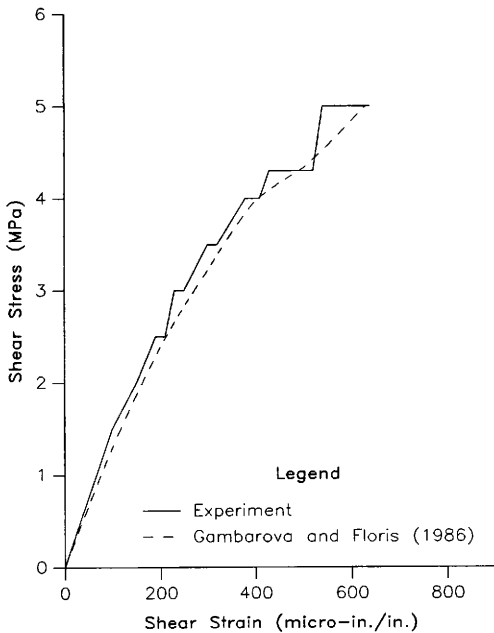
Fig. 45. Response of Hollow Cylinder to Proportional Compressive—Torsional Loading (Gambarova and Floris 1986).
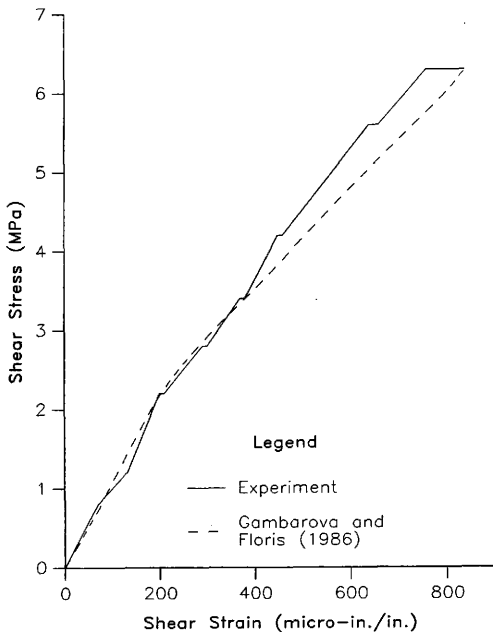
(6.895 MPa = 1 ksi)

Fig. 46. Response of Hollow Cylinder to Sequential Compressive—Torsional Loading (Gambarova and Floris 1986).

(6.895 MPa = 1 ksi)

in which compressive strain softening is incorporated in the microplane model. Another limitation is that the model has no failure criterion. To solve this problem, the stiffness normal to a microplane may be dropped to zero when the normal strain on that plane exceeds a given value. A third limitation of the microplane model may be the scale of the problem under consideration. For example, the one−way slab is a scaled down model of the prototype slab. It is unknown whether the microplane model would predict the same failure load for the prototype as for the model.

In addition to the limitations of the microplane model, limitations to use of ABAQUS, version 4.5, exist. One limitation is the number of microplanes which may be used in an analysis. When 24 microplanes were used, it was observed that ABAQUS lost some of the variables or stored the variables in the wrong locations. However, the same analysis with 12 microplanes ran perfectly. Another limitation is the step size. At critical points such as limit loads, several iterations may be needed. It was observed that ABAQUS sometimes chooses incremental strains $\Delta\epsilon_{ij}$ which cause microplanes to errantly unload from compression or tension, which leads to numerical instablilities. An example of such a situation is uniaxial tension, where the peak value of stress is the critical point. To solve this problem, small load increments should be taken at or near the critical point. Also, the Riks method significantly helps in obtaining a solution free of numerical instabilities.

Recommendations

Among the many concrete material models proposed recently, the plastic−fracturing model, the endochronic model, and microplane model appear to be three promising models which merit further investigation. Given the outlines of each model sketched here, more research should be done to directly compare results of the three models for the same structure. This would allow quantification of the

accuracy of each model for a given problem. For larger structures such as dams, nuclear reactors, bridge girders, and offshore structures, research should be done to determine the necessary parameters to obtain the fracture energy to model crack propagation. Further research should be done to study the interaction between reinforcing steel and concrete.

REFERENCES

[1]   ACI 318–83 (1983). "Building Code Requirements for Reinforced Concrete." ACI Committee 318, American Concrete Institute, Detroit, Michigan.

[2]   Aktan, A.E., and Pecknold, D.A. (1975). "Response of a Reinforced Concrete Section to Two-Dimensional Curvature Histories." *Journal of the American Concrete Institute*, 71(5), 246–250.

[3]   Allen, D.H. (1988). "Introduction to the Mechanics of Elastoplastic and Viscoplastic Media." Aerospace Engineering Department, Texas A & M University. College Station , Texas, unpublished course notes.

[4]   Allen, D.H., Harris, C.E., and Groves, S.E. (1987). "Damage Modelling in Laminated Composites." *Proceedings of the IUTAM/ICM Symposium on Yielding, Damage and Failure of Anisotropic Solids.*

[5]   Argyris, J.H., Faust, F., Szimmat, J., Warnke, E.P., and Willam, K.J. (1974). "Recent Developments in the Finite Element Analysis of Prestressed Concrete Reactor Vessels." *Nuclear Engineering and Design*, 28, 42–75.

[6]   Batdorf, S.B., and Budiansky, B. (1949). "A Mathmatical Theory of Plasticity Based on the Concept of Slip." NACA TN1871, April.

[7]   Bažant, Z.P. (1980). "Work Inequalities for Plastic Fracturing Materials." *International Journal of Solids and Structures*, 16, 873–901.

[8]   Bažant, Z.P. (1984). "Microplane Model for Strain–Controlled Inelastic Behavior." *Mechanics of Engineering Materials.* C.S. Desai and R.H. Gallagher, eds., John Wiley and Sons, Inc., 45–59.

[9]   Bažant, Z.P. (1987). "Fracture Energy of Heterogeneous Materials and Similitude." SEM/RILEM International Conference on Fracture of Concrete and Rock, eds. S.P. Shah and S.E. Swartz, Houston, Texas, June, 390–402.

[10] Bažant, Z. P. and Cedolin, L. (1979). "Blunt Crack Band Propagation in Finite Element Analysis." *Journal of the Engineering Mechanics Division*, ASCE, 105(EM2), 297–315.

[11] Bažant, Z.P., and Cedolin, L. (1980). "Fracture Mechanicis in Reinforced Concrete." *Journal of the Engineering Mechanics Division*, ASCE, 106(EM6), 1287–1306; discussion by David Darwin and Robert Dodds (1982), 108(EM2), 464–466; Closure, 108(EM2), 466–471.

[12] Bažant, Z.P. and Cedolin, L. (1983). "Finite Element Modeling of Crack Band Propagation." *Journal of Structural Engineering*, ASCE, 109(1), 69–92.

[13] Bažant, Z.P., and Gambarova, G. (1984). "Crack Shear in Concrete: Crack Band Microplane Model." *Journal of Structural Engineering*, ASCE, 110(9), 2015–2035.

[14] Bažant, Z.P., and Kim, S.S. (1979). "Plastic–Fracturing Theory for Concrete." *Journal of the Engineering Mechanics Division*, ASCE, 106(EM3), 407–428.

[15] Bažant, Z.P. and Oh, B.H. (1983A). "Microplane Model for Fracture Analysis of Concrete Structures." *Symposium Proceedings: The Interaction of Non–Nuclear Munitions with Structures*, U.S. Air Force Academy, Colorada, May 10-13, 49–55.

[16] Bažant, Z.P. and Oh, B.H. (1983B). "Efficient Numerical Integration on the Surface of a Sphere." Report No. 83–2/428e, Center for Concrete and Geomaterials, Northwestern University, Evanston, Ill.

[17] Bažant, Z. P. and Oh, B. H. (1985). "Microplane Model for Progressive Fracture of Concrete and Rock." *Journal of Engineering Mechanics*, 111(4), 559–582.

[18] Bažant, Z.P., Pan, J., and Pijaudier–Cabot, G. (1987). "Softening in Reinforced Concrete Beams and Frames." *Journal of the Structural Division*, ASCE, 113(12), 2333–2347.

[19] Bažant, Z.P., and Shieh, C.L. (1978). "Endochronic Model for Nonlinear Triaxial Behavior of Concrete." *Nuclear Engineering and Design*, 47, 305–315.

[20] Bell, J.C., and Elms, D.G. (1971)., "A Finite Element Approach to Post Elastic Slab Behavior." *American Concrete Institute Special Publication*, SP30–15, 325–344.

[21] Blakely, F.A., and Beresford, F.D. (1955). "Tensile Strains in Concrete." CSIR *Reports* C2.2 (1,2), Commonwealth Scientific and Industrial Research Organization, Melbourne; Part 2, 52 p.

[22] Blakely, R.W.G., and Park, R. (1973). "Prestressed Concrete Sections with Cyclic Flexure." *Journal of the Structural Division*, ASCE, 99(ST8), 1717–1742.

[23] Buyukozturk, O., (1977). "Nonlinear Analysis of Reinforced Concrete Structures." *Computers and Structures*, 7, 149–156.

[24] Calladine, C.R. (1971). "A Microstructural View of the Mechanical Properties of Saturated Clay." *Geotechnique*, 21, 391–415.

[25] Carino, N.J., and Slate, F.O. (1976). "Limiting Tensile Strain Criterion for Failure of Concrete." *ACI Journal*, 73(3), 160–165.

[26] Carpinteri, A. (1982). "Application of Fracture Mechanics to Concrete Structures." *Journal of the Structural Division*, ASCE, 108(ST4), 833–848.

[27] Cedolin, L., Crutzen, Y.R.J., and Dei Poli, S. (1977). "Triaxial Stress-Strain Relationship for Concrete." *Journal of the Engineering Mechanics Division*, ASCE, 103(EM3), 423–439.

[28] Cervenka, V. and Gerstle, K.H. (1972). "Inelastic Analysis of Reinforced Concrete Panels." *Publications*, International Association for Bridge and Structural Engineering, 32–II, 25–39.

[29] Chang, H.T., and Allen, D.H. (1987). "Predicted Dynamic Response of a Composite Beam with History–Dependent Damage." *Computers and Structures*, 26(4), 575–580.

[30] Chen, A. C. T. and Chen, W. F. (1975). "Constitutive Relations for Concrete." *Journal of the Engineering Mechanics Division, ASCE*, 101(EM4), 465–481.

[31] Chen, W.F. (1981). *Plasticity in Reinforced Concrete*, McGraw–Hill Book Company, New York.

[32] Chen, W.F., and Ting, E.C. (1980). "Constitutive Models for Concrete Structures." *Journal of the Engineering Mechanics Division*, ASCE, 106(EM1), 1–19.

[33] Colville, J., and Abbasi, J. (1974). "Plane Stress Reinforced Concrete Finite Elements." *Journal of the Structural Division*, ASCE, 100(ST5), 1067–1083.

[34] Como, M. and D'Agostino, S. (1969). "Strain–Hardening Plasticity with Baushinger Effect." *MECCANICA : Journal of Italian Association of Theoretical and Applied Mechanics*, AIMETA 2, 146–159.

[35] Cordebois, J. and Sidoroff, F. (1982). "Endommagement Anisotroe." *Journal de Mecanique Theoritique et Appliquee*, Special.

[36] Crisfield, M.A. (1981). "A Fast Incremental/Iterative Solution Procedure that Handles Snap–Through." *Computers and Structures*, 13, 55–62.

[37] Darwin, D., and Pecknold, D.A. (1974). "Inelastic Model for Cyclic Biaxial Loading Of Reinforced Concrete." Civil Engineering Studies, SRS No. 409, University of Illinois at Urbana-Champaign, Urbana, Ill., 169 p.

[38] Darwin, D., and Pecknold, D.A. (1976). "Analysis of Reinforced Concrete Panels Under Cyclic Loading." *Journal of the Structural Division*, ASCE, 102(ST2), 355–369.

[39] De Villiers, I.P. (1977). "Implementation of Endochronic Theory for Analysis of Concrete Structures." Ph.D. Dissertation, University of California, Berkeley.

[40] Donida, G., Floris, C., and Gambarova, P.G. (1987). "An Application of the Microplane Model to the Analysis of Reinforced Concrete Shear Walls." *Constitutive Laws for Engineering Materials : Theory and Applications*, C.S. Desai et al., editors, 841–848.

[41] Doughill, J.W. (1975). "Some Remarks on Path Independence in the Small in Plasticity." *Quarterly Journal of Applied Mathematics*, 32, 233–243.

[42] Doughill, J.W. (1976). "On Stable Progressively Fracturing Solids." *Zeitschrift für Angewandte Mathematik un Physik*, 27(4), 423–437.

[43] Dragon, A., and Mróz, Z. (1979). "A Continuum Model for Plastic–Brittle Behavior of Rock and Concrete." *International Journal of Engineering Sciences*, 17, 121–137.

[44] Evans, R.H., and Marathe, M.S. (1968). "Microcracking and Stress–Strain Curves for Concrete in Tension." *Materials and Structures* , No. 1, January–February, 61–64.

[45] Fanning, D.N., and Dodge, W.G. (1979). "Methods of Calculating Inelastic Response of Prestressed Concrete Pressure Vessels." 5th International Conference on Structural Mechanics in Reactor Technology, W. Berlin.

[46] Gambarova, P.G., and Floris, C. (1986). "Microplane Model for Concrete Subject to Plane Stresses." *Nuclear Engineering and Design*, 97, 31–48.

[47] Gilbert, R.I., and Warner, R.F. (1978). "Nonlinear Analysis of Reinforced Concrete Slabs with Tension Stiffening." *UNICIV* Report No. R–167, School of Civil Engineering, University of New South Wales, Kensington, Australia.

[48] Gopalaratnam, V.S., and Shah, S.P. (1985). "Softening Response of Plain Concrete in Direct Tension." *ACI Journal*, 85(3), 310–323.

[49] Gustaffason, P.J., and Hillerborg, A. (1988). "Sensitivity in Shear Strength of Longitudinally Reinforced Concrete Beams to Fracture Energy of Concrete." *ACI Structural Journal*, 85(3), 286–294.

[50] Hand, F.R., Pecknold, D.A., and Schnobrick, W.C. (1973). "Nonlinear Analysis of R.C. Plates and Shells." *Journal of the Structural Division*, ASCE, 99(ST7), 1491–1505.

[51] Heilmann, H.G. and Hilsdorf, H. (1969). "Strength of Concrete Under Tensile Stress." *Bulletin* No. 203, Deutsher Ausschuss fur Stahlbeton, Berlin, 94 p.

[52] Hibbitt, H.D. (1985). "ABAQUS–EPGEN – A General Purpose Finite Element Code with Emphasis on Nonlinear Applications." *Nuclear Engineering and Design*, 77, 271–298.

[53] Hillerborg, A. (1985). "Numerical Methods to Simulate Softening and Fracture of Concrete." *Fracture Mechanics of Concrete: Structural Application and Numerical Calculation*. Martinus Nijhoff Publishers, Dordrecht, 141–170.

[54] Hsieh, B.J. (1980). "On the Uniqueness and Stability of Endochronic Theory." Report, Argonne National Laboratory Components Technology Division, Argonne, Illinois.

[55] Hsu, T.T.C., Slate, F.O., Sturman, G.M., and Winter, G. (1963). "Microcracking of Concrete and the Shape of the Stress–Strain Curve." *ACI Journal*, 60(2), 209–224.

[56] Hughes, B. P. and Chapman, G. P. (1966). "The Complete Stress-Strain Curve for Concrete in Direct Tension." *RILEM Bull.* 30, 95–97.

[57] Jain, S.C., and Kennedy, J.B. (1974). "Yield Criterion of Reinforced Concrete Slabs." *Journal of the Structural Division*, ASCE, 100(ST3), 631–644.

[58] Jofriet, J.C., and McNiece, G.M. (1971). "Finite Element Analysis of Reinforced Concrete Slabs." *Journal of the Structural Division*, ASCE, 97(ST3), 785–806.

[59] Jones, R. (1968). "Cracking and Failure of Concrete Test Specimens Under Uniaxial Quasi-Static Loading." *Proceedings*, International Conference on the Structure of Concrete, Cement and Concrete Association, London, 125–130.

[60] Kachanov, L.M. (1958). "Time of the Rupture Process Under Creep Condtions." TVZ Akad Nauk S.S.R. Otd Tech. Nauk 8 (cited in Kachanov 1986).

[61] Kachanov, L.M. (1986). *Introduction to Continuum Damage Mechanics*. Martinus Nijhoff Publishers, Boston.

[62] Kaplan, M.F. (1961). " Crack Propagation and the Fracture of Concrete." *ACI Journal*, 58(5), 591–610.

[63] Kaplan, M.F. (1963). "Strains and Stresses of Concrete at Initiation of Cracking and Near Failure." *ACI Journal*, 60(7), 853–879.

[64] Karsan, I.K., and Jirsa, J.O. (1969). "Behavior of Concrete Under Compressive Loadings." *Journal of the Structural Division*, ASCE, 95(ST12), 2543–2563.

[65] Kent, D.C. and Park, R. (1971). "Flexural Members with Confined Concrete." *Journal of the Structural Division*, ASCE, 97(ST7), 1969–1990.

[66] Kesler, C.E., Naus, D.J., and Lott, J.L. (1972). "Fracture Mechanics–Its Applicability to Concrete." *Proceedings of the 1971 International Conference on Mechanical Behavior of Concrete*, Japan, 4, 113–124.

[67] Kotsovos, M.D., and Newman, J.B. (1978). "Generalized Stress-Strain Relations for Concrete." *Journal of the Engineering Mechanics Division*, ASCE, 104(EM4), 845–856.

[68] Krajcinovic, D. (1979). "Distributed Damage Theory of Beams in Pure Bending." *Journal of Applied Mechanics*, 46, September, 592–596.

[69] Krajcinovic, D. (1983). "Constitutive Equations for Damaging Materials." *Journal of Applied Mechanics*. 50, 355–360.

[70] Krajcinovic, D. (1984). "Continuum Damage Mechanics." *Applied Mechanics Reviews*, 37, 397–406.

[71] Kupfer, H.B., and Gerstle, K.H. (1973). "Behavior of Concrete Under Biaxial Stresses." *Journal of the Engineering Mechanics Division*, ASCE, 99(EM4), 852–866.

[72] Kupfer, H.B., Hilsdorf, H.K., and Rüsch, H. (1969). "Behavior of Concrete Under Biaxial Stresses." *Journal of the American Concrete Institute*, 66(8), 656–666.

[73] Lemaitre, J. (1984). "How to Use Damage Mechanics." *Nuclear Engineering and Design*, 80, 233–245.

[74] Lin, C.S., and Scordelis, A.C. (1975). "Nonlinear Analysis of R.C. Shells of General Form." *Journal of the Structural Division*, ASCE, 101(ST3), 523–538.

[75] Malvern, L.E. (1969). *Introduction to the Mechanics of a Continuous Medium*. Prentice Hall, Inc., Englewood Cliffs, N.J.

[76] McHenry, D., and Karni, J. (1958). "Strength of Concrete Under Combined Tensile and Compressive Stress." *ACI Journal*, 54(10), 829–840.

[77] Mindness, S., and Young, J.F. (1981). *Concrete*. Prentice-Hall, Inc., Englewood Cliffs, New Jersey.

[78] Newman, K. (1968). "Criteria for the Behavior of Plain Concrete Under Complex States of Stress." *Proceedings*, International Conference on the Structure of Concrete, Cement and Concrete Association, London, 255–274.

[79] Ngo, D., and Scordelis, A.C. (1967). "Finite Element Analysis of Reinforced Concrete Beams." *Journal of the American Concrete Institute*, 64(3), 152–163.

[80] Nishizawa, N. (1961). "Strength of Concrete Under Combined Tensile and Compressive Loads." *Review of the Fifteenth General Meeting*, Japan Cement Engineering Association, Tokyo, 242–245.

[81] Ottosen, N.S. (1977). "A Failure Criterion for Concrete." *Journal of the Engineering Mechanics Division*, ASCE, 103(EM4), 527–535.

[82] Ottosen, N.S. (1979). "Constitutive Model for Short–Time Loading of Concrete." *Journal of the Engineering Mechanics Division*, ASCE, 105(EM1), 127–141.

[83] Palaniswamy, R., and Shah, S.P. (1974). "Fracture and Stress–Strain Relation of Concrete Under Triaxial Compression." *Journal of the Strucural Division*, 100(ST5), 901–916.

[84] Phillips, D.V., and Zienkiewicz, O.C. (1976). "Finite Element Nonlinear Analysis of Concrete Structures." *Proceedings*, The Institution of Civil Engineers, 61, Part 2, 59–88.

[85] Ramaley, D., and McHenry, D. (1947). "Stress–Strain Curves for Concrete Strained Beyond the Ultimate Load." Laboratory Report No. SP12, U.S. Bureau of Reclamation.

[86] Ramm, E. (1981). "Strategies for Tracing the Nonlinear Response Near Limit Points." *Nonlinear Finite Element Analysis in Structural Mechanics*, Proceedings of the Europe–U.S. Workshop Ruhr Universtat Bochrum, Germany, Eds. W. Wunderlich, E. Stein, and K.J. Bathe, 63–86.

[87] Rashid, Y.R. (1968). "Ultimate Strength Analysis of Prestressed Concrete Pressure Vessels." *Nuclear Engineering and Design*, 7.

[88] Rashid, Y.R., and Dunham, R.S. (1986). "Three–Dimensional Constitutive Model for the Analysis of Concrete Stuctures." Anatech International Corporation Report No. ANA–86–0052, July.

[89] Reinhardt, H.W. (1985). "Plain Concrete Modeled as an Elastic Strain–Softening Material at Fracture." *Engineering Fracture Mechanics*, 22(5), 787–796.

[90] Riks, E. (1979). "An Incremental Approach to the Solution of Snapping and Buckling Problems." *International Journal of Solids and Structures*, No. 7–B, 529–551.

[91] Robinson, G.S. (1967). "Behavior of Concrete in Biaxial Compression." *Proceedings*, ASCE, 93(STI), 71–86.

[92] Roelfstra, P.E. and Wittman, F.H. (1985). "Numerical Method to Link Strain–Softening Failure of Concrete." *Proceedings*, International Conference on Fracture Mechanics of Concrete, Elsevier, Amsterdam, 127–139.

[93] Rosenthal, I. (1968). "Strength of Plain Concrete Under Two–Dimensional Combined Stresses." DS Thesis, Technion–Israel Institute of Technology, Haifa, (in Hebrew, with English summary).

[94] Rüsch, H. (1960). "Research Toward a General Flexural Theory for Structural Concrete." *Journal of the American Concrete Institute*, 57(1), 1–23.

[95] Scanlon, A., (1971). "Time Dependent Deflections of Reinforced Concrete Slabs." Thesis presented to the University of Albert, at Edmonton, Alberta, Canada, in partial fulfillment of the requirements for the degree of Doctor of Philosophy.

[96] Seaman, L., Curran, D.R., and Shockley, D.A. (1976). "Computational Models for Ductile and Brittle Fracture." *Journal of Applied Physics*, 47(11), 4814–4826.

[97] Sinha, B.P., Gerstle, K.H., and Tulin, L.G. (1964). "Stress–Strain Relations for Concrete Under Cyclic Loading." *Journal of the American Concrete Institute*, 62(2), 195–211.

[98] Slate, F.O., and Meyers, B.L. (1968). "Deformations of Plain Concrete." *Proceedings*, Fifth International Symposium on the Chemistry of Cement, Tokyo; Part III, Properties of Cement Paste and Concrete, 142–151.

[99] Smith, G.M. (1953). "Failure of Concrete Under Combined Tensile and Compressive Stresses." *ACI Journal*, 50(2), 137–140.

[100] Sorenson, S.I., Arneson, A, and Bergan, P.G. (1978). "Nonlinear Finite Element Analysis of Reinforced Concrete using Endochronic Theory." *Finite Elements in Nonlinear Mechanics*, Tapir, Norwegian Institute of Technology, Trondheim, 1, 167–190.

[101] Stroud, A.H. (1971). *Approximate Calculation of Multiple Integrals*, Prentice Hall, Englewood Cliffs, N.J.

[102] Suharwardy, M.I.H., and Pecknold, D.A. (1978). "Inelastic Response of Reinforced Concrete Columns Subjected to Two–Dimensional Earthquake Motions." Civil Engineering Studies, SRS No. 455, University of Illinois at Urbana-Champaign, Urbana, Ill., October, 210 pp.

[103] Suidan, M. and Schnobrich, W.C. (1973). "Finite Element Analysis of Reinforced Concrete." *Journal of the Structural Division*, ASCE, 99(ST10), 2109–2122.

[104] Tasuji, M.E., Slate, F.O., and Nilson, A.H. (1978). "Stress–Strain Response and Fracture of Concrete in Biaxial Loading." *ACI Journal*, 75(7), 306–312.

[105] Taylor, G.I. (1938). "Plastic Strain in Metals." *Journal for the Institute for Metals*, 62, 307–324.

[106] Tamuzh, V. and Lagsdinsh, A. (1968). "Variant of Fracture Theory." *Journal of Mechanics of Polymers*, (in Russian), Riga, No. 4.

[107] Wanchoo, M.K., and May, G.W. (1975). "Cracking Analysis of Reinforced Concrete Plates." *Journal of the Structural Division*, 101(ST1), 201–215.

[108] Weigler, H., and Becker, G. (1963). "Brush and Verformungsverhalten von Beton bei Zweiachsiger Beanspruchung." *Bulletin* No. 157, Deutscher Ausschuss fur Stahlbeton, Berlin, 66 p.

[109] Willam, K.J., and Warnke, E.P. (1974). "Constitutive Model for the Triaxial Behavior of Concrete." International Association of Bridge and Structural Engineers, Seminar on Concrete Structures Subjected to Triaxial Stresses, Paper III-1, Bergama, Italy, May 17–19.

[110] Winter, G., and Nilson, A.H. (1979). *Design of Concrete Structures*. ninth edition, McGraw-Hill Book Company, New York, 16.

[111] Wu, T.T., and Drucker, D.C. (1967). "Continuum Plasticity Theory in Relation to Solid Solution, Dispersion, and Precipitation Hardening." *Journal of Applied Mechanics*, 34, 195–199.

[112] Yankelevsky, D.Z., and Reinhardt, H.W. (1987). "Response of Plain Concrete to Cyclic Tension." *ACI Materials Journal*, 84(5), 365–373.

[113] Zhen–Hai, G., and Xiu–Qin, Z. (1987). "Investigation of Complete Stress-Deformation Curves for Concrete in Tension." *ACI Materials Journal*, 84(4), 278–285.

[114] Zienkiewicz, O.C., and Pande, G.N. (1977). "Time–Dependent Multi-Laminate Model of Rocks – A Numerical Study of Deformation and Failure of Rock Masses." *International Journal of Numerical and Analytical Methods in Geomechanics*, 1, 219–247.

VITA

James Harris Loper was born in Atlanta, Georgia, and raised in Decatur, Georgia. He graduated from Towers High School in Decatur in 1982. His higher education consisted of B.S. and M.S. degrees in 1986 and 1988, respectively, from Texas A & M University, College Station, Texas. His major subject was Civil Engineering. He is a member of Triangle Fraternity, Phi Kappa Phi, Tau Beta Pi, and Chi Epsilon. He will begin a professional career on September 1, 1988, with Lockwood Greene Engineers, Inc., in Atlanta, Georgia. He now resides at 1775 Lee Street, Decatur, Georgia 30035.